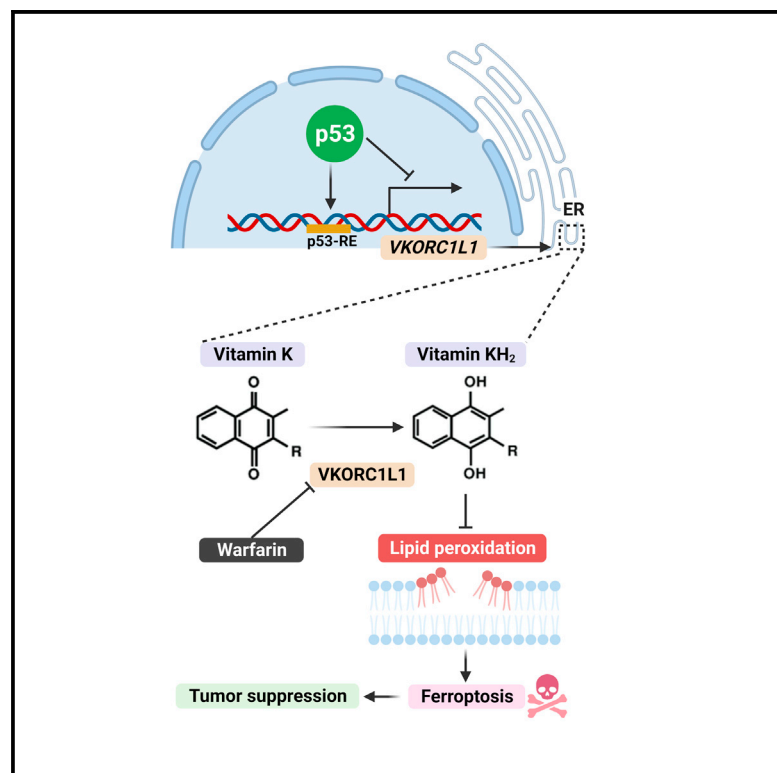# Regulation of VKORC1L1 is critical for p53-mediated tumor suppression through vitamin K metabolism

Graphical abstract

Highlights

- VKORC1L1 is a potent ferroptosis suppressor

- VKORC1L1 catalyzes the reduced form of vitamin K to counteract phospholipid peroxides

- p53 transcriptionally represses VKORC1L1 expression to activate ferroptosis

- Targeting VKORC1L1 by warfarin promotes ferroptosis and tumor suppression *in vivo*

Authors

Xin Yang, Zhe Wang,
Fereshteh Zandkarimi, ...,
Xuejun Jiang,
Brent R. Stockwell, Wei Gu

Correspondence

wg8@cumc.columbia.edu

In brief

Yang et al. found the canonical vitamin K cycle reductase VKORC1L1, which catalyzes the reduced form of vitamin K to protect cells from ferroptosis. Suppression of VKORC1L1 either by p53 through transcription or by pharmacological inhibition by warfarin activates ferroptosis and induces tumor suppression *in vivo*.

CellPress

Cell Metabolism

CellPress

Regulation of VKORC1L1 is critical for p53-mediated tumor suppression through vitamin K metabolism

Xin Yang,[1,8] Zhe Wang,[1,8] Fereshteh Zandkarimi,[2,3] Yanqing Liu,[1] Shoufu Duan,[1] Zhiming Li,[1] Ning Kon,[1] Zhiguo Zhang,[1,4] Xuejun Jiang,[5] Brent R. Stockwell,[2,6] and Wei Gu[1,7,9,*]

[1]Institute for Cancer Genetics, and Herbert Irving Comprehensive Cancer Center, Vagelos College of Physicians & Surgeons, Columbia University, New York, NY, USA
[2]Department of Chemistry, Columbia University, New York, NY, USA
[3]Mass Spectrometry Core Facility, Columbia University, New York, NY, USA
[4]Department of Pediatrics, and Department of Genetics and Development, Vagelos College of Physicians & Surgeons, Columbia University, New York, NY, USA
[5]Cell Biology Program, Memorial Sloan-Kettering Cancer Center, New York, NY, USA
[6]Department of Biological Sciences, Columbia University, New York, NY, USA
[7]Department of Pathology and Cell Biology, Vagelos College of Physicians & Surgeons, Columbia University, New York, NY, USA
[8]These authors contributed equally
[9]Lead contact
*Correspondence: wg8@cumc.columbia.edu
https://doi.org/10.1016/j.cmet.2023.06.014

SUMMARY

Here, we identified vitamin K epoxide reductase complex subunit 1 like 1 (VKORC1L1) as a potent ferroptosis repressor. VKORC1L1 protects cells from ferroptosis by generating the reduced form of vitamin K, a potent radical-trapping antioxidant, to counteract phospholipid peroxides independent of the canonical GSH/GPX4 mechanism. Notably, we found that VKORC1L1 is also a direct transcriptional target of p53. Activation of p53 induces downregulation of VKORC1L1 expression, thus sensitizing cells to ferroptosis for tumor suppression. Interestingly, a small molecular inhibitor of VKORC1L1, warfarin, is widely prescribed as an FDA-approved anticoagulant drug. Moreover, warfarin represses tumor growth by promoting ferroptosis in both immunodeficient and immunocompetent mouse models. Thus, by downregulating VKORC1L1, p53 executes the tumor suppression function by activating an important ferroptosis pathway involved in vitamin K metabolism. Our study also reveals that warfarin is a potential repurposing drug in cancer therapy, particularly for tumors with high levels of VKORC1L1 expression.

INTRODUCTION

The main feature of ferroptosis is the accumulation of excessive lipid peroxides, which causes cellular membrane dysfunction and cell death.[1] Cells undergo the following two major mechanisms of inducing lipid peroxidation: autoxidation and enzymatically catalyzed oxidation.[2] Acyl-coenzyme A (CoA) synthetase long-chain family member 4 (ACSL4) and peroxisomes contribute to the synthesis of phosphatidylethanolamine (PE) or ether phospholipids (ePLs) with polyunsaturated fatty acyl tails (PUFAs), which act as the major substrate for lipid peroxidation to drive ferroptosis.[3–5] Although autoxidation is predominant in the generation of lipid peroxides, enzymatic lipid peroxidation carried out by lipoxygenase family proteins (ALOXs) also plays an indispensable role in pathology in some cases.[6] For example, ALOX12 is critical for p53-mediated tumor suppression by promoting ferroptosis.[7,8] ALOX15-catalyzed lipid peroxidation occurs in asthma, kidney injury, and brain trauma, and ALOX5 is particularly important for ferroptotic responses in the striatal neurons from Huntington's disease mice.[9,10]

Conversely, the mechanisms of eliminating lipid peroxides are also crucial for ferroptosis. GPX4 was initially identified as the major protein directly detoxifying lipid peroxides into non-toxic lipid alcohol by using glutathione (GSH).[11] The cellular GSH synthesis pathway and cystine transporter system x_c^- are essential for GPX4-mediated ferroptosis prevention. In addition, several mechanisms independent of GSH/GPX4 have been shown to eliminate lipid peroxides and inhibit ferroptosis. Ferroptosis suppressor protein 1 (FSP1, encoded by *AIFM2*) and dihydroorotate dehydrogenase (DHODH) convert CoQ_{10} to $CoQ_{10}H_2$, a kind of radical-trapping antioxidant (RTA), to decrease the lipid peroxides in different subcellular compartments.[12–14] Tetrahydrobiopterin (BH_4), metabolized by GTP cyclohydrolase 1 (GCH1) and dihydrofolate reductase (DHFR), also acts as an RTA to counteract lipid peroxidation.[15,16] The calcium-independent phospholipase iPLA2β cleaves hydroperoxide acyl tails from phospholipids to inhibit ferroptosis.[17,18] Notably, vitamin K is the most recently reported metabolite that can potently inhibit ferroptosis.[19] FSP1, the CoQ_{10} reductase enzyme, surprisingly also mediates the reduction of vitamin K, which is responsible
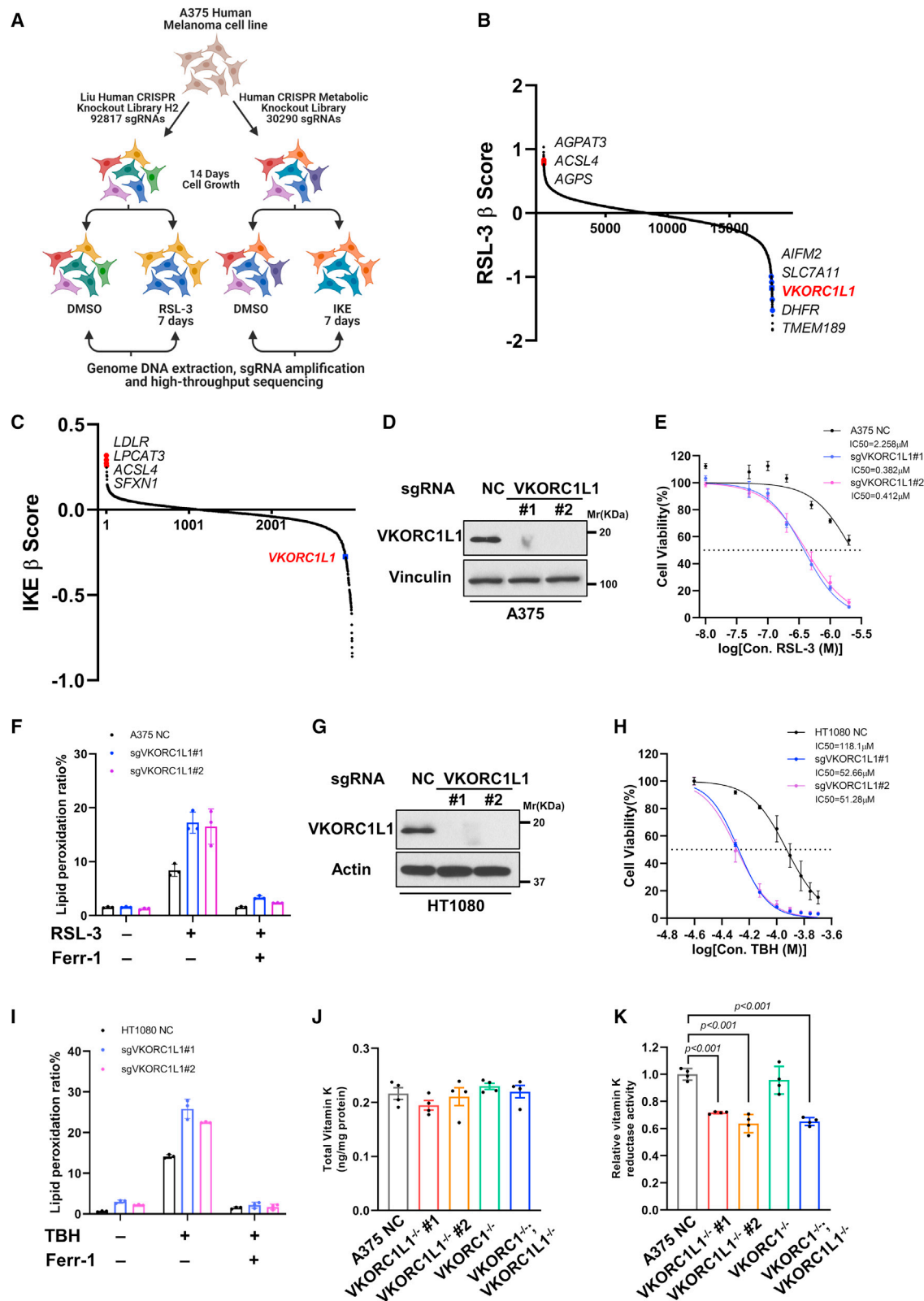
Figure 1. CRISPR-Cas9 screening identified *VKORC1L1* as a potent ferroptosis suppressor

(A) Schematic of the CRISPR screening workflow in human melanoma A375 cells by human genome-wide CRISPR knockout library under RSL-3 treatment or by human metabolic CRISPR knockout library under IKE treatment.

(legend continued on next page)

Cell Metabolism
Article

CellPress

for suppressing ferroptosis.[20] Nevertheless, it remains unclear whether FSP1 is the only enzyme responsible for this anti-ferroptosis pathway. More importantly, given the role of ferroptosis in modulating tumor growth, it will be interesting to know whether vitamin K metabolism is connected with major tumor suppression pathways in vivo.

In this study, we performed CRISPR-Cas9 knockout screens and identified vitamin K epoxide reductase complex subunit 1 like 1 (VKORC1L1) as a critical contributor to ferroptosis surveillance. VKORC1L1 enzymatically reduced vitamin K to generate vitamin K hydroquinone, a potent RTA, to eliminate lipid peroxides. We revealed that mevalonate-derived pathways are critical for fueling vitamin K synthesis and showed that VKORC1L1 is a major target of p53 during tumor suppression in a GSH-independent manner. Notably, treating cells with warfarin, a well-known VKORC1L1 inhibitor, resulted in tumor suppression in vivo by promoting ferroptosis. Thus, these data elucidate a previously unanticipated pathway for p53-mediated tumor suppression through vitamin K metabolism and also raise a possibility of repurposing warfarin, an anti-thrombotic drug, for treating the tumors with high levels of VKORC1L1 expression.

RESULTS

The CRISPR-Cas9 screening identified *VKORC1L1* as a potent ferroptosis suppressor

To uncover the intrinsic metabolisms that modulate the susceptibility of cells to ferroptosis, we performed a genetic screen in human melanoma A375 cells using a CRISPR-Cas9 genome-wide gene knockout library. To this end, cells infected with the indicated library were selected by puromycin and cultured for an additional 14 days. Surviving cells with or without treatment with RSL-3, a potent GPX4 inhibitor, were collected, and their sgRNA abundance was sequenced and analyzed using model-based analysis of genome-wide CRISPR-Cas9 knockout (MAGeCK) (Figure 1A).[21] Well-known ferroptosis inducers *ACSL4*, *AGPAT3*, and *AGPS* were uncovered, suggesting the robustness of the screen. Among the genes that promoted ferroptosis after being knocked out, the top hits included *AIFM2*, *DHFR*, and *SLC7A11*, which are known ferroptosis regulators (Figure 1B). Interestingly, a vitamin K metabolic gene, *VKORC1L1*, showed a similar β score as *SLC7A11* (−1.17 for

VKORC1L1 versus −1.07 for *SLC7A11*), suggesting a potential role of *VKORC1L1* against ferroptosis (Figures 1B and S1A). In addition, *VKORC1L1* was also identified as a top hit in the screen with a metabolic gene knockout library. Under the condition of prolonged GSH depletion induced by imidazole ketone erastin (IKE) treatment, *VKORC1L1* also appeared among the top hits of genes (Figures 1C and S1B). Hence, both CRISPR-Cas9 screens identified *VKORC1L1* as a potential ferroptosis suppressor.

To evaluate the effect of VKORC1L1 during ferroptosis, we generated VKORC1L1-knockout A375 cells by the CRISPR-Cas9 technique (Figure 1D). Cells with depleted VKORC1L1 expression showed significant decreases in cell viability and increases in lipid peroxidation under RSL-3 treatment at different time points (8, 12, 24, and 48 h), validating the results from the CRISPR-Cas9 knockout screen (Figures 1E, 1F, and S1C–S1E). VKORC1L1-knockout cells also showed reduced levels of cell viability after IKE- or cystine-deficient-mediated GSH depletion treatment (Figures S1F and S1G). Furthermore, we deleted VKORC1L1 in fibrosarcoma HT1080 cells (Figure 1G). Consistent with the results in A375 cells, knocking out VKORC1L1 in HT1080 cells resulted in dramatically decreased cell viability levels and increased lipid peroxidation levels after treating cells with RSL-3 or cystine-deficient medium (Figures S1H–S1O). Interestingly, VKORC1L1 was required for cell survival during the treatment with tert-butyl hydroperoxide (tBuOOH, TBH), a reactive oxygen species (ROS) radical generator that can promote ferroptosis independent of ACSL4 (Figures 1H and 1I).[7,18] These data indicate that VKORC1L1 inhibits ferroptosis through reducing lipid peroxidation.

VKORC1L1 is a key player in the canonical vitamin K cycle and has a similar function as vitamin K epoxide reductase complex subunit 1 (VKORC1). Both enzymes are involved in reducing vitamin K epoxide to vitamin K and reducing vitamin K to vitamin K hydroquinone.[22] However, these two enzymes apparently have distinct roles in embryonic development.[23] In addition, vitamin K-dependent gamma-carboxylase (GGCX) mediates the carboxylation of vitamin K-dependent proteins by converting the vitamin K hydroquinone to vitamin K epoxide (Figure S2A). Although *VKORC1* and *GGCX* apparently showed no obvious effect in both RSL-3- and IKE-mediated ferroptosis based on the results from our screens (Figures 1B and 1C), we assessed

---

(B) Plot showing the β scores (RSL-3 versus DMSO) for all targeted genes by human genome-wide CRISPR knockout library. Red or blue dots indicate significantly positive or negative selected genes, respectively, which have already been identified as key regulators in ferroptosis.

(C) Plot showing the β scores (IKE versus DMSO) for all targeted genes by human metabolic CRISPR knockout library. Red or blue dots indicate significantly positive or negative selected genes, respectively, which have already been identified as key regulators in ferroptosis.

(D) Western blot analysis of A375 cells expressing negative control sgRNA (sgNC, referred as NC) or VKORC1L1-targeted sgRNA (sgVKORC1L1, referred as VKORC1L1$^{-/-}$).

(E) Cell viability of A375 NC or two VKORC1L1$^{-/-}$ clones treated with RSL-3 for 8 h.

(F) Lipid peroxidation ratio of NC or two VKORC1L1$^{-/-}$ clones A375 cells treated with RSL-3 (400 nM) and ferrostatin-1 (5 µM) for 4 h.

(G) Western blot analysis of HT1080 cells expressing negative control sgRNA (sgNC, referred as NC) or VKORC1L1-targeted sgRNA (sgVKORC1L1, referred as VKORC1L1$^{-/-}$).

(H) Cell viability of HT1080 NC or two VKORC1L1$^{-/-}$ clones treated with TBH for 6 h.

(I) Lipid peroxidation ratio of HT1080 NC or two VKORC1L1$^{-/-}$ clones treated with TBH (100 µM) and ferrostatin-1 (5 µM) for 4 h.

(J) Total vitamin K levels of A375 NC, two VKORC1L1$^{-/-}$ clones, VKORC1$^{-/-}$, and VKORC1$^{-/-}$; VKORC1L1$^{-/-}$ cells.

(K) Relative vitamin K reductase activity. Relative abundance of MK4H$_2$ production by incubating MK4 with whole-cell proteins of A375 NC, two VKORC1L1$^{-/-}$ clones, VKORC1$^{-/-}$, and VKORC1$^{-/-}$; VKORC1L1$^{-/-}$ analyzed by LC-MS.

For (E), (F), (H), and (I), data are the mean ± SD of n = 3, and for (J) and (K), data are the mean ± SD of n = 4 independent biological repeats. p values were calculated using unpaired, two-tailed Student's t test.

(legend on next page)

Cell Metabolism
Article

CellPress
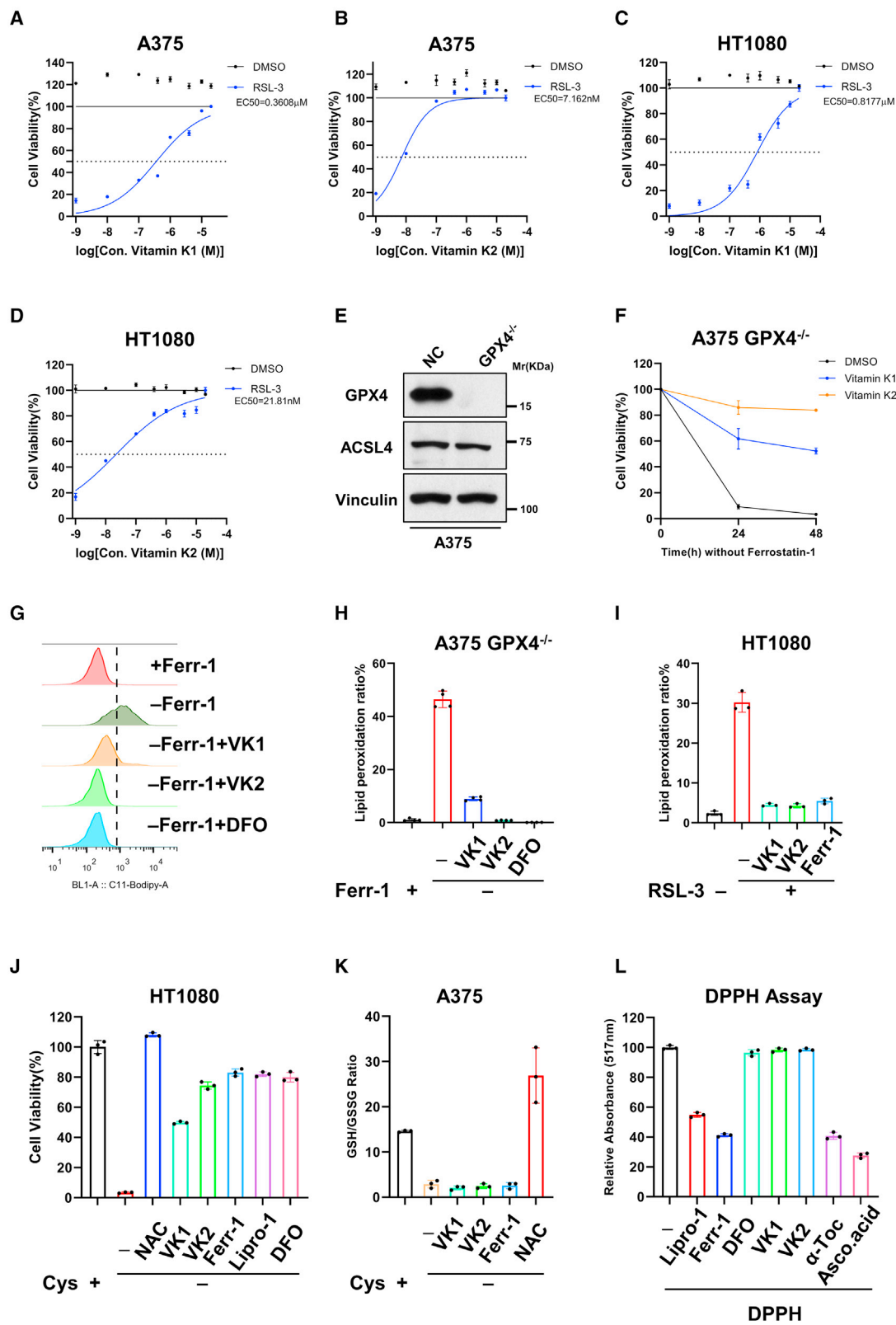
their roles in ferroptosis by using VKORC1- or GGCX-knockout cells. As expected, loss of either VKORC1 or GGCX expression by the transfection of corresponding sgRNAs in A375 cells did not sensitize the cells to ferroptosis (Figures S2B–S2D). To further evaluate the role of VKORC1 in ferroptosis, we established the VKORC1/VKORC1L1 double-null A375 cells (Figure S2E) to find that the loss of VKORC1 modestly enhanced the sensitivity of the VKORC1L1-null cells in ferroptosis (Figures S2F and S2G). Conversely, VKORC1 overexpression only partially blocked the high levels of ferroptosis response in the VKORC1L1-null cells (Figures S2H and S2I). These data suggest that although both VKORC1 and VKORC1L1 catalyze the same enzymatic reaction to produce the reduced forms of vitamin K, VKORC1L1 plays a much more dominant role than VKORC1 in the anti-ferroptosis effects.

Next, we examined the effects of VKORC1L1 in regulating the levels of the reduced form of vitamin K. As expected, the levels of the total vitamin K were unchanged by the loss of VKORC1L1 (Figures 1J and S2J). By using the method developed by the Conrad lab to examine the role of FSP1 in catalyzing the reaction between oxidized and reduced form of one type of vitamin K2 (menaquinone 4 [MK4]) (referred to as MK4 and MK4H$_2$, respectively),[20] we tested whether VKORC1L1 is critical for generating the reduced form of vitamin K (Figure S2K). As shown in Figure 1K, the levels of MK4H$_2$ production in VKORC1L1-knockout cells were significantly decreased in comparison to the control cells; in contrast, loss of VKORC1 had negligible effects on MK4H$_2$ production. Loss of both VKORC1L1 and VKORC1 (the VKORC1L1/VKORC1-double-knockout cells) did not further reduce the levels of MK4H$_2$ as shown in the VKORC1L1-null cells. Consistently, overexpression of VKORC1 only had very modest effects on the levels of the reduced form of vitamin K shown in the VKORC1L1-null cells (Figure S2L). Thus, these results suggest that VKORC1L1 is the major enzyme for producing the reduced form of vitamin K.

Vitamin K exhibits anti-ferroptosis functions in a GSH-independent manner

To further dissect the role of VKORC1L1 in regulating ferroptosis, we examined whether the ferroptosis response in cells is affected by vitamin K treatment. To this end, HT1080 and A375 cells were treated with a lethal dose of RSL-3 together with vitamin K, and the cell viability was determined. The results showed that both bioactive vitamin K, phylloquinone (vitamin K1) and MK4 (vitamin K2) exerted potent ferroptosis protection activities (Figures 2A–2D). Similar results were also obtained in the cells treated with IKE or TBH (Figures S3A and S3B). Next, we tested the role of vitamin K in spontaneous ferroptosis upon the loss of endogenous GPX4 (Figure 2E). Indeed, spontaneous ferroptosis in GPX4-null cells was largely suppressed by the treatment with vitamin K (Figures 2F and S3C). Consistently, the levels of the lipid peroxides were also reduced by the same treatment (Figures 2G–2I).

We further examined the role of vitamin K in modulating ferroptosis under different settings. As shown in Figure 2J, the ferroptosis response upon cystine starvation was also suppressed by vitamin K treatment (Figures 2J, S3D, and S3E). Interestingly, vitamin K treatment reduced the levels of lipid peroxidation but had no effects on the intracellular GSH concentration or the GSH/GSSG ratio (Figures 2K, S3F, and S3G), suggesting that the vitamin K-mediated protection against ferroptosis is GSH independent. Moreover, mouse hippocampal neuronal HT22 cells are used widely in evaluating glutamate-induced oxidative stress that is caused by inhibiting cystine import.[24] Indeed, glutamate treatment caused decreases in the viability of HT22 cells, which was attenuated by vitamin K and other canonical ferroptosis inhibitors (Figures S3H and S3I). In addition, vitamin K treatment also reduced the levels of lipid peroxidation induced by glutamate (Figure S3J), indicating that vitamin K is a bona fide ferroptosis inhibitor. Nevertheless, vitamin K displayed no radical-scavenging capacity in in vitro 2,2-diphenyl-1-picrylhydrazyl (DPPH) assay (Figure 2L), suggesting a metabolite of vitamin K, but not vitamin K itself, reacts with free radicals. Moreover, vitamin K is different from the known ferroptosis-protective metabolites (vitamin E, BH$_4$, BH$_2$, and ubiquinol) but is similar to ubiquinone (Figure S3K).[25] Taken together, our results demonstrate that vitamin K is a unique ferroptosis inhibitor, independent of the canonical GSH/GPX4 repressive pathway.

VKORC1L1 mediates anti-ferroptosis effects by promoting vitamin K hydroquinone generation

Next, we evaluated the anti-ferroptosis effects of VKORC1L1 following vitamin K treatment. As shown in Figures 3A and 3B, loss of VKORC1L1 significantly reduced the effects of vitamin

---

Figure 2. Vitamin K exhibits anti-ferroptosis functions in a GSH-independent manner

(A and B) Cell viability assay for evaluating the protective effects of vitamin K1 (A) or vitamin K2 (B) against RSL-3 (1 μM)-induced ferroptosis in A375 cells for 8 h.

(C and D) Cell viability assay for evaluating the protective effects of vitamin K1 (C) or vitamin K2 (D) against RSL-3 (300 nM)-induced ferroptosis in HT1080 cells for 8 h.

(E) Western blot analysis of A375 NC and GPX4$^{-/-}$ cells.

(F) Cell viability assay for evaluating the protective effects of vitamin K1 or vitamin K2 in A375 GPX4$^{-/-}$ cells with ferrostatin-1 withdrawn for periods of time as indicated.

(G and H) Lipid peroxidation measurement (G) and ratio (H) of vitamin K1 (10 μM), vitamin K2 (5 μM), or deferoxamine (DFO) (50 μM) treatment in A375 GPX4$^{-/-}$ cells, with ferrostatin-1 withdrawn for 4 h.

(I) Lipid peroxidation ratio of HT1080 cells under RSL-3 (250 nM) with vitamin K1 (10 μM), vitamin K2 (5 μM), or ferrostatin-1 (5 μM) treatment for 4 h.

(J) Cell viability levels of wild-type HT1080 cells cultured in cystine-deficient medium with NAC (400 μM), vitamin K1 (10 μM), vitamin K2 (5 μM), ferrostatin-1 (5 μM), liproxstatin-1 (5 μM), or DFO (50 μM) treatment for 24 h.

(K) Intracellular GSH/GSSG ratio of A375 cells cultured in cystine-deficient medium with vitamin K1 (10 μM), vitamin K2 (5 μM), ferrostatin-1 (5 μM), or NAC (400 μM) treatment for 24 h.

(L) In vitro DPPH assay for evaluating the ability of radical-trapping antioxidants (RTAs); ferrostatin-1 (5 μM) and liproxstatin-1 (5 μM) are positive controls. Vitamin K1 (5 μM), vitamin K2 (5 μM), DFO (50 μM), α-tocopherol (5 μM), or ascorbic acid (5 μM) was used.

For (A)–(D), (F), and (I)–(L), data are the mean ± SD of n = 3, and for (H), data are the mean ± SD of n = 4 independent biological repeats.
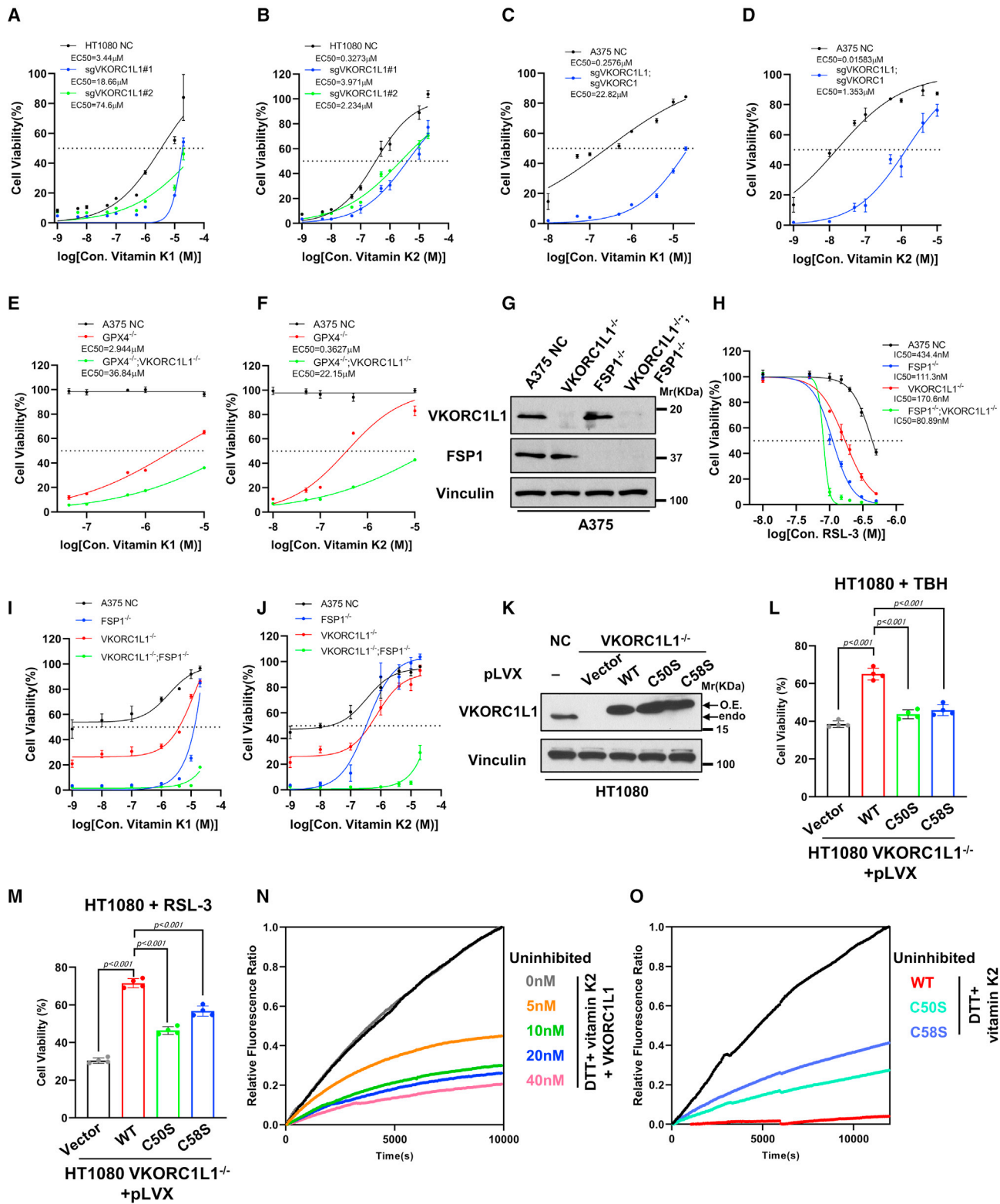
Figure 3. VKORC1L1 mediates anti-ferroptosis effects by promoting vitamin K hydroquinone generation
(A and B) Cell viability assay for evaluating the protective effects of vitamin K1 (A) or vitamin K2 (B) against RSL-3 (250 nM)-induced ferroptosis in HT1080 NC and two VKORC1L1$^{-/-}$ clones for 48 h.
(C and D) Cell viability assay for evaluating the protective effects of vitamin K1 (C) or vitamin K2 (D) against RSL-3 (1 μM)-induced ferroptosis in A375 NC and VKORC1L1$^{-/-}$; VKORC1$^{-/-}$ cells for 48 h.

(legend continued on next page)

Cell Metabolism
Article

CellPress

K in the ferroptosis protection in the HT1080 cells. Similar results were also obtained in VKORC1L1/VKORC1 double-null cells, suggesting that VKORC1L1 is required for the ferroptosis inhibitory effects induced by vitamin K treatment (Figures 3C and 3D). Moreover, we also tested the effects on the ferroptosis that occurred in GPX4-null cells (Figures S4A and S4B). Again, loss of VKORC1L1 significantly reduced the sensitivity of vitamin K in the ferroptosis, induced by the loss of GPX4 (Figures 3E and 3F). Taken together, these data suggest that VKORC1L1 is required for vitamin K-mediated anti-ferroptotic effects. Of note, the treatment with vitamin K in VKORC1L1/VKORC1-double-null cells, at a very high dosage, is still able to exert protective effects against ferroptosis, supporting the notion that additional factors such as FSP1 may play a similar role as VKORC1L1 in vivo.[20]

To further characterize the role of VKORC1L1, we generated FSP1-null and VKORC1L1/FSP1 double-null A375 cells (Figure 3G). As expected, the levels of ferroptosis were significantly increased in either FSP1-null cells or VKORC1L1-null cells upon RSL-3 treatment (Figure 3H); notably, the VKORC1L1/FSP1 double-null A375 cells showed much higher levels of ferroptosis than the FSP1-null cells or VKORC1L1-null cells (Figure 3H). Next, we tested whether these isogenic cells showed different sensitivities for ferroptosis inhibition by vitamin K. To this end, RSL-3-induced ferroptosis was treated with vitamin K1 or vitamin K2 to examine the anti-ferroptosis activities of vitamin K in the absence of VKORC1L1 or/and FSP1. As expected, loss of either VKORC1L1 or FSP1 partially abrogated the anti-ferroptosis effects by either vitamin K1 or vitamin K2 (Figures 3I and 3J); interestingly, the anti-ferroptosis effects by either vitamin K1 or vitamin K2 were severely diminished in the VKORC1L1/FSP1 double-null A375 cells (Figures 3I and 3J) even under high concentrations of vitamin K, suggesting that both VKORC1L1 and FSP1 are required for the anti-ferroptosis effects by vitamin K. These data indicate that VKORC1L1 and FSP1 are not redundant and act independently in ferroptosis protection.

VKORC1L1 contains two conserved cysteines (Cys-50 and Cys-58) that transfer two electrons to the active sites (Cys-142 and Cys-139, respectively). Both these two conserved cysteines are essential for VKORC1L1 reduction activities (Figure S4C).[26] Then, we examined whether these enzymatic mutants are able to rescue the activity of VKORC1L1 in ferroptosis protection in VKORC1L1-null cells (Figure 3K). Indeed, wild-

type VKORC1L1, but not the functional mutants, was able to rescue the cell death upon TBH- or RSL-3 treatment (Figures 3L and 3M). Consistently, these two mutants failed to effectively decrease the levels of lipid peroxidation (Figure S4D).

Next, we examined if VKORC1L1-mediated vitamin K reduction is directly involved in reducing lipid peroxides. As shown in Figure S4E, the lipophilic STY-BODIPY autoxidation is initiated by 2,2′-azobis(2-methylpropionamidine) dihydrochloride (AAPH)-derived radicals that could be reduced by RTAs.[27,28] Because DTT can chemically reduce vitamin K to vitamin K hydroquinone,[29] we optimized the ratio of DTT and vitamin K to minimize the effects. As shown in Figure 3N, a combination of DTT and vitamin K2 showed negligible effects on autoxidation (gray line versus black line), while significant inhibition was observed by adding as little as 5 nM recombinant VKORC1L1 proteins (orange line versus black line), demonstrating that the activities of VKORC1L1 are required for inhibiting lipid peroxidation. The inhibiting effects of VKORC1L1 were dose dependent (Figure 3N). In addition, the rates of inhibiting autoxidation were dependent on the concentrations of both vitamin K1 and vitamin K2 (Figures S4F and S4G). Furthermore, VKORC1L1 C50S and C58S mutants showed decreased inhibitory activities compared with wild type (Figure 3O), demonstrating that vitamin K hydroquinone produced by VKORC1L1 is the bioactive RTA for directly inhibiting lipid peroxidation.

Further characterization of vitamin K-mediated anti-ferroptosis effects

To further investigate the role of vitamin K in regulating ferroptosis, we examined the role of key factors involved in vitamin K production. As shown in Figure 4A, phylloquinone is a vegetable-derived vitamin K that undergoes side-chain changing processes to generate mammalian-consumed vitamin K2. Prenyltransferase UBIAD1 catalyzes the conversion of menadione to MK4 by using geranylgeranyl pyrophosphate (GGPP), a metabolic intermediate from the mevalonate pathways.[30] Indeed, overexpression of UBIAD1 was able to suppress ferroptosis by decreasing lipid peroxidation levels (Figures 4B–4D). As expected, vitamin K levels were increased upon UBIAD1 overexpression in both wild-type cells and VKORC1L1-null A375 cells, validating the role of UBIAD1 in promoting vitamin K production (Figures 4E and 4F).

Given the requirements of GGPP during the UBIAD1-mediated vitamin K synthesis, we next focused on the mechanism by

(E and F) Cell viability assay for evaluating the protective effects of vitamin K1 (E) or vitamin K2 (F) in A375 GPX4$^{-/-}$ or GPX4$^{-/-}$; VKORC1L1$^{-/-}$ cells, with ferrostatin-1 withdrawn for 48 h.

(G) Western blot analysis of A375 NC, VKORC1L1$^{-/-}$, FSP1$^{-/-}$, and VKORC1L1$^{-/-}$; FSP1$^{-/-}$ cells.

(H) Cell viability of A375 NC, VKORC1L1$^{-/-}$, FSP1$^{-/-}$, and VKORC1L1$^{-/-}$; FSP1$^{-/-}$ cells treated with RSL-3 for 8 h.

(I and J) Cell viability assay for evaluating the protective effects of vitamin K1 (I) or vitamin K2 (J) against RSL-3 (250 nM)-induced ferroptosis in A375 NC, VKORC1L1$^{-/-}$, FSP1$^{-/-}$, and VKORC1L1$^{-/-}$; FSP1$^{-/-}$ cells for 24 h.

(K) Western blot analysis of HT1080 NC and VKORC1L1$^{-/-}$ cells re-expressing empty vector, VKORC1L1 WT, VKORC1L1 C50S mutant, or VKORC1L1 C58S mutant.

(L and M) Cell viability levels of HT1080 VKORC1L1$^{-/-}$ cells re-expressing empty vector, VKORC1L1 WT, VKORC1L1 C50S mutant, or VKORC1L1 C58S mutant with TBH (100 μM, L) or RSL-3 (100 nM, M) treatment for 6 h.

(N) Relative STY-BODIPY autoxidation rate by tittered purified VKORC1L1 proteins in the presence of vitamin K2 (20 μM) and DTT (500 μM).

(O) Relative STY-BODIPY autoxidation rate by purified wild type, C50S mutant, or C58S mutant VKORC1L1 proteins in the presence of vitamin K2 (20 μM) and DTT (500 μM).

For (A)–(F) and (H)–(J), data are the mean ± SD of n = 3, and for (L) and (M), data are the mean ± SD of n = 4 independent biological repeats. p values were calculated using unpaired, two-tailed Student's t test.
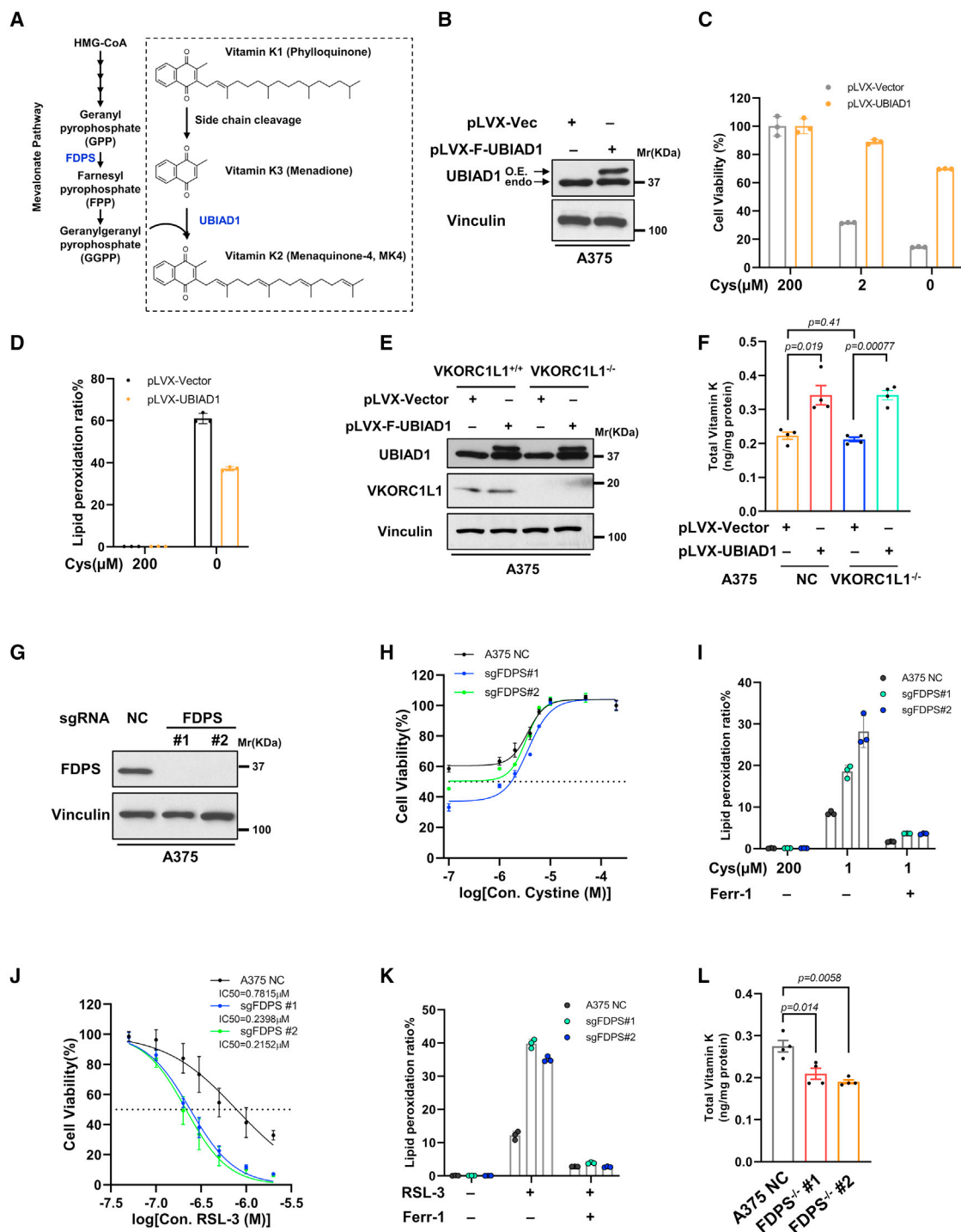
Figure 4. Further characterization of vitamin K-mediated anti-ferroptosis effects

(A) Model of UBIAD1-mediated vitamin K side-chain transferring. Phytyl group on plant-derived phylloquinone (vitamin K1) is first cleaved to generate menadione (vitamin K3). The prenyltransferase UBIAD1 converts menadione to menaquinones (vitamin K2, MK4) by using geranylgeranyl diphosphate (GGPP) synthesized from the mevalonate pathway. FDPS is the rate-limiting enzyme for FPP generation, which provides the substrate for GGPP generation.

(B) Western blot analysis of A375 overexpressing empty vector or UBIAD1 cells.

(C) Cell viability levels of A375 overexpressing empty vector or UBIAD1 cells cultured under medium with indicated cystine concentration for 24 h.

(D) Lipid peroxidation ratio of A375 overexpressing empty vector or UBIAD1 cells cultured without or with cystine-deficient medium for 12 h.

(E) Western blot analysis of A375 NC or VKORC1L1$^{-/-}$ cells re-overexpressing empty vector or UBIAD1.

(F) Total vitamin K levels of A375 NC re-overexpressing empty vector, VKORC1L1$^{-/-}$ re-overexpressing empty vector, NC re-overexpressing UBIAD1, or VKORC1L1$^{-/-}$ re-overexpressing UBIAD1 cells.

Cell Metabolism
Article

CellPress

which the mevalonate pathway modulates the sensitivity of cells to ferroptosis (Figure S4H).[31,32] Notably, from the top hits in our CRISPR-Cas9 screens, we found that farnesyl pyrophosphate synthase (FDPS) is a top candidate for the ferroptosis repressor (Figures S4I and S4J). FDPS-mediated farnesyl diphosphate (FPP) generation is the rate-limiting step for GGPP generation.[33] As expected, CRISPR-mediated deletion of FDPS decreased the levels of cell viability and increased the levels of lipid peroxidation under cystine starvation or RSL-3 treatment (Figures 4G–4K). Moreover, the treatment of FDPS-null cells with the FPP supplement significantly rescued the cells from ferroptosis (Figure S4K), suggesting that the enzymatic activity of FDPS in FPP production is critical. In addition, loss of FDPS expression also decreased the production of the total vitamin K levels (Figure 4L). These results indicate the critical roles of the mevalonate pathway and the FDPS-UBIAD1 axis in ferroptosis defense through vitamin K production.

VKORC1L1 is a direct transcriptional repression target of p53

Upon analysis of p53 chromatin immunoprecipitation (ChIP) sequencing data,[34,35] p53 is found enriched in the *VKORC1L1* promoter region, indicating that p53 may be involved in VKORC1L1 transcriptional regulation. We first examined the *VKORC1L1* mRNA expression upon p53 activation by treating cells with Nutlin or doxorubicin in p53 wild-type cells. *VKORC1L1* mRNA levels were significantly decreased in p53 wild-type A375 and U2OS cells upon both treatments (Figures 5A and S5A). In contrast, the decrease of *VKORC1L1* mRNA and protein levels was mostly abrogated in CRISPR-mediated *p53*-null A375 and U2OS cells (Figures 5B–5D and S5B). In fact, the expression levels of VKORC1L1 were increased in p53-knockout cells, indicating that p53 was required to regulate the basal levels of VKORC1L1 (Figures 5B–5D and S5B). Meanwhile, p53 activation downregulated VKORC1L1 levels in a time-dependent manner (Figures 5E and S5C). Similar results were obtained from mouse embryonic fibroblasts (MEFs), further validating the p53-mediated *Vkorc1l1* transcriptional repression in mouse cells (Figure S5D). Notably, in *p53*-null H1299 cells, *VKORC1L1* mRNA levels were decreased by the overexpression of wild-type p53, but not transcription-deficient p53 mutants, including R175H, R273H, and R248W (Figure S5E), suggesting that the p53-mediated *VKORC1L1* transcriptional repression depends on its intact DNA-binding domain. It has been reported that most p53-mediated transcriptional repression acts indirectly through either p21 activation or microRNA processing.[36,37] To evaluate whether *VKORC1L1* is a direct target, we generated CRISPR-mediated p21 and DGCR8-double-knockout HCT116 cells where the repression through p21 activation or microRNA processing is abolished (Figure S5F). Strikingly, p53-mediated

repression of *VKORC1L1* remained intact in those cells (Figure 5F), suggesting that VKORC1L1 is a direct target of p53.

To further assess the direct regulatory role of p53 on VKORC1L1, we analyzed the ChIP-seq data and found a significant occupancy of human p53 on the *VKORC1L1* promoter region that contains potential consensus p53-binding sequence (Figure S5G). Indeed, ChIP-qPCR assay showed that p53 had a dramatic enrichment on *VKORC1L1* promoter but not on control IgG both in A375 and HCT116 cells (Figures 5G and S5H). Similar ChIP-seq and ChIP-qPCR results were obtained from MEFs (Figures 5H and S5I). To validate whether this p53-binding sequence confers p53-dependent transcriptional repression, we cloned the DNA fragment into a firefly luciferase reporter (Figures S5J and S5K). p53 suppressed the luciferase expression driven by the *VKORC1L1* reporter construct containing p53-binding sequence, and more importantly, mutations at the p53-binding site largely abrogated p53-mediated repression (Figure 5I). Together, these data demonstrate that the *VKORC1L1* is a bona fide repression target of p53.

p53-mediated ferroptosis acts at least, in part, through vitamin K metabolism

To elucidate the functional consequence of the transcriptional repression of VKORC1L1 by p53, we examined the effects of vitamin K in p53-dependent ferroptosis. Indeed, p53 activation by Nutlin significantly reduced the sensitivity of vitamin K in suppressing ferroptosis (Figures 6A, 6B, S6A, and S6B). Moreover, p53-mediated repression of VKORC1L1 also decreased the levels of the reduced form of vitamin K (Figures S6C and S6D), providing direct evidence for p53 in modulating vitamin K metabolism. To further understand the consequence of the p53-VKORC1L1 regulation, we examined p53 responses in VKORC1L1-knockout cells and found that loss of VKORC1L1 had no effect on p53 levels and p53-mediated transcription (Figure 6C). As expected, p53-null cells were resistant to ferroptosis, whereas loss of VKORC1L1 sensitized the cells to ferroptosis (Figures 6D and 6E).

To further elucidate the role of VKORC1L1 in p53-mediated ferroptosis, we tested whether ectopic expression of VKORC1L1 is able to modulate ferroptotic responses induced by p53. To this end, VKORC1L1 was expressed in both native A375 cells and isogenic p53-null A375 cells (Figure S6E). The high levels of ferroptosis in native A375 cells were abrogated upon VKORC1L1 expression (Figure S6F). On the other hand, loss of p53 largely diminished the sensitivity of ferroptosis in p53-null A375 cells; more importantly, no obvious effect on the levels of ferroptosis was detected upon the expression of VKORC1L1 in p53-null A375 cells under the same conditions (Figure S6F). Next, we examined whether ectopic expression of VKORC1L1 was able to suppress p53-mediated tumor

(G) Western blot analysis of A375 cells expressing negative control sgRNA (sgNC) or FDPS targeted sgRNA (sgFDPS).

(H) Cell viability of A375 sgNC or two sgFDPS clones under medium with indicated cystine concentration for 24 h.

(I) Lipid peroxidation ratio of A375 sgNC or two sgFDPS clones cultured with indicated cystine concentration and ferrostatin-1 (5 μM) for 12 h.

(J) Cell viability of A375 sgNC or two sgFDPS clones treated with RSL-3 for 8 h.

(K) Lipid peroxidation ratio of A375 sgNC or two sgFDPS clones treated with RSL-3 (400 nM) and ferrostatin-1 (5 μM) for 4 h.

(L) Total vitamin K levels of A375 sgNC or two sgFDPS clones.

For (C), (D), and (H)–(K), data are the mean ± SD of n = 3, and for (F) and (L), data are the mean ± S.D. of n = 4 independent biological repeats. p values were calculated using unpaired, two-tailed Student's t test.
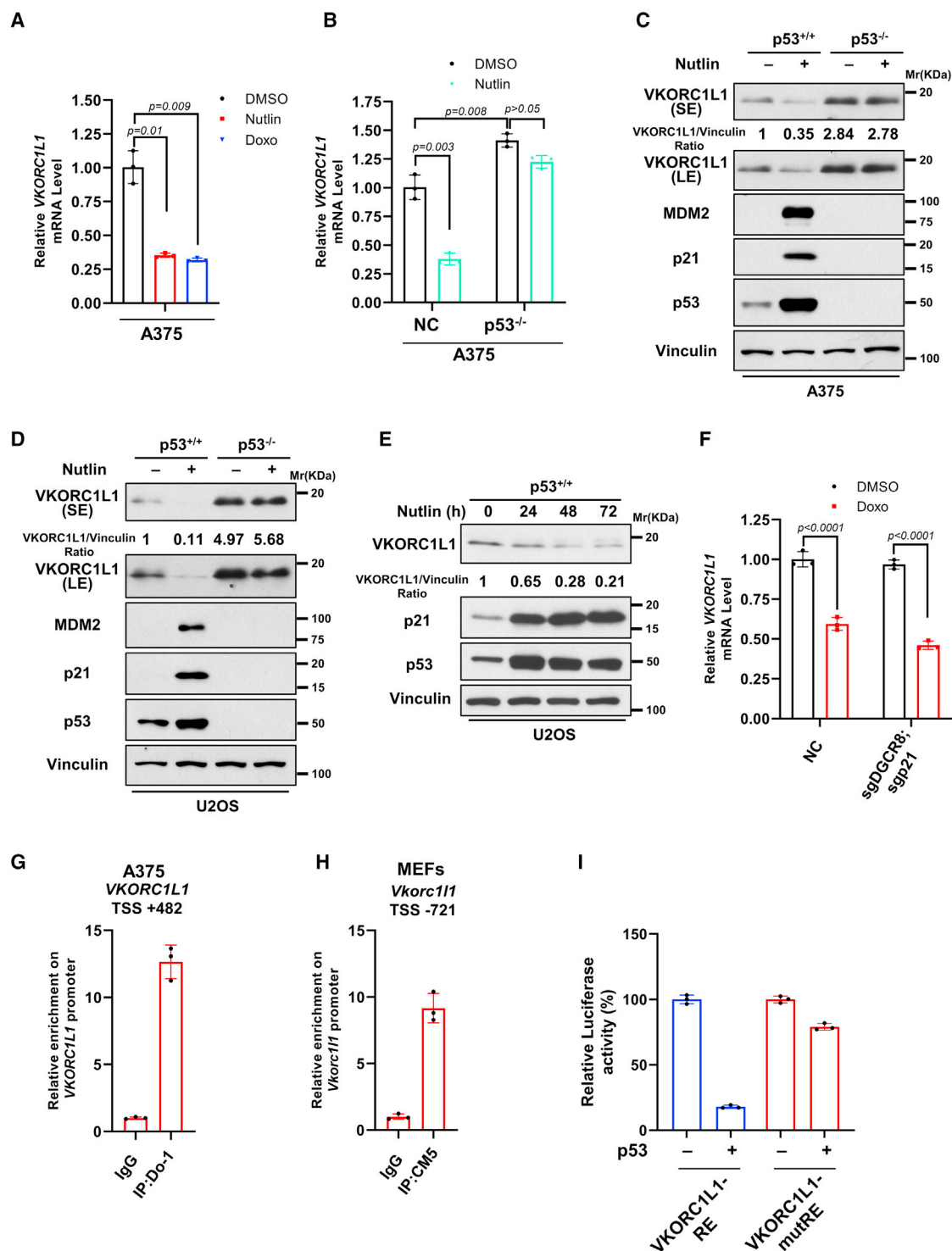
Figure 5. VKORC1L1 is a direct transcriptional repression target of p53

(A) Quantitative real-time PCR analysis of mRNA levels of *VKORC1L1* in A375 cells treated with DMSO, 10 μM Nutlin-3, or 0.2 μg/mL doxorubicin for 24 h.

(B) Quantitative real-time PCR analysis of mRNA levels of *VKORC1L1* in A375 NC or p53$^{-/-}$ cells treated with DMSO or 10 μM Nutlin-3 for 36 h.

(C) Western blot analysis of A375 NC and p53$^{-/-}$ cells treated with DMSO or 10 μM Nutlin-3 for 48 h. MDM2 and p21 are positive controls.

(D) Western blot analysis of U2OS NC and p53$^{-/-}$ cells treated with DMSO or 10 μM Nutlin-3 for 48 h. MDM2 and p21 are positive controls.

(E) Western blot analysis of U2OS cells under 10 μM Nutlin-3 treatment with indicated time. p21 is a positive control.

(F) Quantitative real-time PCR analysis of mRNA levels of *VKORC1L1* in HCT116 NC and sgDGCR8; sgp21 HCT116 cells treated with DMSO or 10 μM Nutlin-3 for 24 h.

Cell Metabolism
Article

CellPress

suppression by using xenograft tumor models. As shown in Figures 6F and 6G, overexpression of VKORC1L1 significantly abrogated the tumor growth suppression in p53 wild-type A375 tumors, whereas no obvious effect was observed in isogenic p53-null A375 tumors. By using fluorescence-activated cell sorting (FACS) analysis of the levels of lipid peroxidation derived from the fresh tumors, we further validated that the expression of VKORC1L1 significantly suppressed the ferroptosis response in the p53 wild-type A375 tumors, but not in p53-null A375 tumors (Figure 6H).

The upregulation of *VKORC1L1* mRNA and protein levels in p53-null cells also suggests the potential clinical significance of *VKORC1L1* in tumors induced by *p53* genomic alteration. Indeed, by analyzing the data from the UCSC Xeno platform,[38] we found that *VKORC1L1* expression is upregulated in patients who harbored *p53* mutants among PanCancer Atlas (PAN), colon adenocarcinoma (COAD), and stomach adenocarcinoma (STAD) (Figures S6G–S6I). Moreover, although *VKORC1L1* amplification rates in PanCancer are as low as 1%, notably shorter overall survival is observed for patients with *VKORC1L1* genomic amplification, compared with the survival of patients with unaltered *VKORC1L1* genomic composition (Figure 6I), highlighting that the high expression of *VKORC1L1* predicts poor outcome.

Targeting vitamin K cycle by warfarin promotes ferroptosis and tumor suppression *in vivo*

Given that the high expression of VKORC1L1 in patients with mutated p53 predicts poor survival, unleashing the anti-ferroptosis effect by VKORC1L1 may have therapeutic potential. Interestingly, a small molecular inhibitor of VKORC1L1 called warfarin is widely prescribed as an FDA-approved anticoagulant drug (reference ID: 4101432, https://www.accessdata.fda.gov/drugsatfda_docs/label/2011/009218s107lbl.pdf). Thus, it is very likely that warfarin is able to promote ferroptosis by inhibiting VKORC1L1. However, the warfarin-mediated effect is also complexed by the fact that both VKORC1L1 and VKORC1 can be inhibited by warfarin. VKORC1 is inhibited at a low concentration of warfarin, whereas the inhibition of VKORC1L1 requires much higher levels of the drug.[39,40] As discussed above, our data showed that although both VKORC1 and VKORC1L1 are able to catalyze the same enzymatic reaction, VKORC1L1 plays a much more dominant role than VKORC1 in the anti-ferroptosis effects. Indeed, warfarin treatment at low concentrations (0.1–10 μM) showed no obvious effect in ferroptosis responses as only VKORC1 is inhibited under these conditions (Figure S7A). Conversely, high levels of ferroptosis were induced upon warfarin treatment at high concentrations (25–100 μM) (Figure S7A). Indeed, the ferroptosis-enhancing effects of warfarin were largely abrogated by the loss of VKORC1L1, suggesting that VKORC1L1 is the key target of warfarin in sensitizing cells to ferroptosis (Figure S7B). These data further prompted us to investigate the potential clinical significance of warfarin usage in cancer therapy. Previous studies illustrate that warfarin

is associated with a significant improvement in overall survival in COAD, STAD, and pancreatic adenocarcinoma (PAAD) compared with low-molecular-weight heparin (LMWH) or direct oral anticoagulants (DOACs).[41,42] LMWH and DOACs are newly popular anticoagulants that directly inhibit vitamin K-dependent proteins (factors II, VII, and IX) without affecting VKOR enzymes. By analyzing clinical data from the TCGA (The Cancer Genome Atlas) database,[43] we found that *VKORC1L1* is overexpressed in COAD, STAD, and PAAD (Figure S7C). Notably, lower *VKORC1L1* expression corresponds to longer survival probability in pancreatic cancer patients (Figure S7D). We speculated that pancreatic cancer patients may benefit from warfarin usage beyond alleviating thromboembolic diseases.

To this end, we examined the enzymes among the vitamin K cycle and well-known ferroptosis regulators in a series of pancreatic cancer cell lines by western blot assay. VKORC1L1 showed dramatically high expression levels in PANC1 and AsPC1 cells (Figure 7A). By treating cells with vitamin K, we found that vitamin K largely rescued the cystine-deprivation-induced cell death in pancreatic cancer cells that had been identified as preferred models in exploring ferroptosis function in tumor suppression (Figure S7E).[44] Cell toxicity experiments showed that pancreatic cells displayed no proliferation inhibition by warfarin as high as 100 μM (Figure S7F) and over 25 μM warfarin treatment significantly promoted the cell death of AsPC1 cells (Figure S7G). Indeed, warfarin sensitized all pancreatic cancer cells to ferroptosis (Figures 7B–7E and S7H–S7M). Specifically, PANC1 and AsPC1 cells, which had higher VKORC1L1 expression than those of the other cell lines, displayed the largest IC50 differences between warfarin-treated and DMSO-treated cells, suggesting that the high-expression VKORC1L1 is a potential pathological marker for warfarin-mediated effects.

To further strengthen our hypothesis of using warfarin in treating pancreatic cancer, we tested whether warfarin treatment affects tumor growth in a xenograft nude mouse model by using AsPC1 cells. Three groups of mice were supplied with regular water, water containing 1 mg/kg warfarin, or 2 mg/kg warfarin for 15 days. As shown in Figure S7N, warfarin treatment only had slight effects on the mice's weight in the 2 mg/kg warfarin group. Indeed, tumor growth was reduced in both warfarin-treated groups compared with the control group (Figures 7F–7H). The mRNA levels of *PTGS2* were dramatically upregulated in tumors from warfarin-treated tumor tissues (Figure 7I). Consistently, tumor-derived live cells from two warfarin-treated groups displayed dramatically increased lipid peroxidation levels (Figures 7J and 7K). Furthermore, we tested the tumor suppression effects of warfarin by using immunocompetent mice. We established a pancreatic tumor model by using KPCY cells derived from Kras$^{LSL-G12D/+}$; Trp53$^{LSL-R172H/+}$; Pdx1-Cre; Rosa26$^{YFP/YFP}$ mouse.[45] Mice were under 1 mg/kg warfarin administration orally for 15 days. As is shown in Figures S7O–S7Q, warfarin administration decreased the growth of PDAC tumors. Furthermore, we found that the lipid peroxidation levels of

---

(G) ChIP-qPCR analysis of p53 enrichment by DO-1 antibody at *VKORC1L1* promoter region (TSS + 482) in A375 cells treated with 0.4 μg/mL doxorubicin for 24 h.

(H) ChIP-qPCR analysis of p53 enrichment by CM5 antibody at *Vkorc1l1* promoter region (TSS-721) in MEF cells treated with 0.4 μg/mL doxorubicin for 24 h.

(I) Luciferase reporter assay of constructs containing VKORC1L1-RE or VKORC1L1-mutRE in H1299 cells without or with p53 expression vector. *Renilla* control reporter was used as a transfection internal control.

Data are mean ± SD of n = 3 independent biological repeats. p values were calculated using unpaired, two-tailed Student's t test.
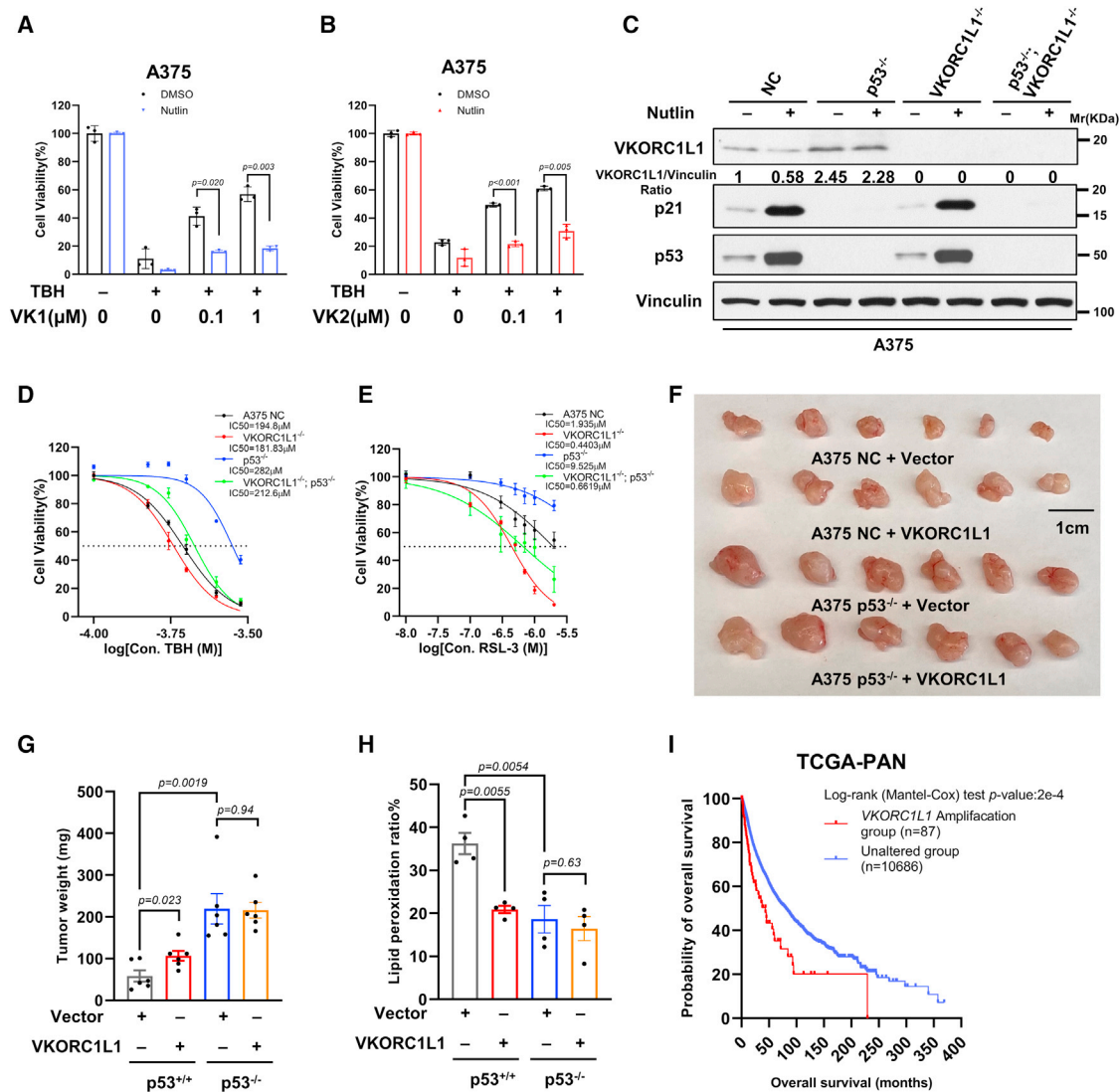
Figure 6. p53-mediated ferroptosis acts at least in part through vitamin K metabolism

(A and B) Cell viability assay for evaluating the protective effects of vitamin K1 (A) or vitamin K2 (B) against TBH (300 μM)-induced ferroptosis for 8 h in A375 cells that were pretreated with 10 μM Nutlin-3 for 24 h.

(C) Western blot analysis of A375 NC, p53$^{-/-}$, VKORC1L1$^{-/-}$, or p53$^{-/-}$; VKORC1L1$^{-/-}$cells treated with DMSO or 10 μM Nutlin-3 for 24 h. p21 is a positive control.

(D) Cell viability of A375 NC, p53$^{-/-}$, VKORC1L1$^{-/-}$, or p53$^{-/-}$; VKORC1L1$^{-/-}$cells pretreated with 10 μM Nutlin-3 for 24 h, then under TBH treatment for 8 h.

(E) Cell viability of A375 NC, p53$^{-/-}$, VKORC1L1$^{-/-}$, or p53$^{-/-}$; VKORC1L1$^{-/-}$ cells treated with RSL-3 for 8 h.

(F) Xenograft tumors presentation of A375 NC or p53$^{-/-}$ cells re-overexpressing empty vector or VKORC1L1-derived tumors. Scale bars, 1 cm.

(G) Tumor weights were determined from (F).

(H) Lipid peroxidation ratio of live cells derived from tumors from (F).

(I) Kaplan-Meier survival curve for overall survival by patient samples within TCGA PanCancer Atlas Studies from cBioPortal based on the genomic status of *VKORC1L1*: amplification (n = 87) and unaltered (n = 10,686).

For (A), (B), (D), and (E), data are mean ± SD of n = 3, and for (H), data are mean ± SD of n = 4 independent biological repeats. For (G), data are mean ± SEM of n = 6 independent tumor samples. For (A), (B), and (H), p values were calculated using unpaired, two-tailed Student's t test. For (G), p values were calculated using one-way ANOVA.

the tumor cells were significantly increased by warfarin treatment, indicating that warfarin contributed to tumor suppression by increasing lipid peroxidation *in vivo* (Figure S7R).

To examine whether the tumor suppressive effects of warfarin require its ability to promote ferroptosis, we tested the effects of warfarin in tumor growth in the absence or presence of ferropto-

sis inhibitor, ferrostatin-1. As expected, warfarin administration significantly suppressed tumor growth (Figures 7L–7N); however, the tumor growth suppressive effects induced by warfarin were largely abrogated upon ferrostain-1 treatment (Figures 7L–7N). Moreover, FACS analysis of the fresh tumor samples revealed that warfarin administration significantly increased the levels of
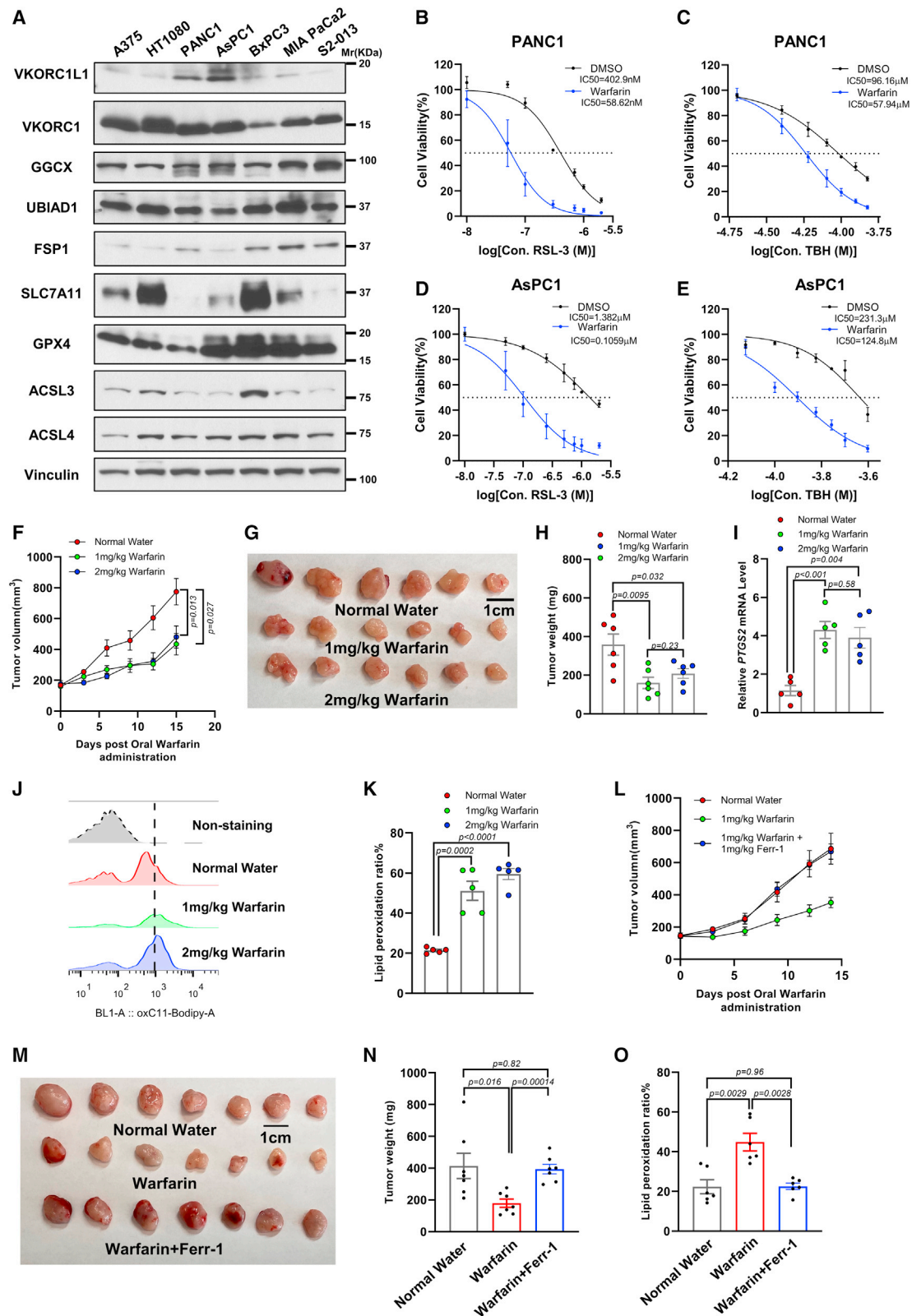
Figure 7. Targeting vitamin K cycle by warfarin promotes ferroptosis and tumor suppression *in vivo*

(A) Western blot analysis of A375, HT1080, PANC1, AsPC1, BxPC3, MIAPaCa2, and S2-013 cells by detecting vitamin K cycle enzymes and known ferroptosis regulators.

lipid peroxidation levels for ferroptosis (Figure 7O). In contrast, the increased levels of lipid peroxidation levels were completely abrogated upon the co-treatment with ferrostatin-1. These results demonstrate that warfarin-induced ferroptosis significantly contributes to its effect on tumor growth suppression *in vivo*. GPX4 protein levels showed negligible changes among these three groups, indicating that warfarin-mediated ferroptosis induction *in vivo* does not act through modulating GPX4 protein expression (Figure S7S). We further detected the total vitamin K levels within tumors and found that endogenous total vitamin K levels were not affected by either warfarin or ferrostatin-1 (Figure S7T). Taken together, these results demonstrate that warfarin suppresses tumor growth in both immunodeficient and immunocompetent pancreatic tumor mouse models by promoting ferroptosis.

DISCUSSION

The role of vitamin K in coagulants has been described for over 85 years, and coagulant factor carboxylation is considered the major function of the vitamin K cycle. Here, we demonstrate the unexpected function of the vitamin K cycle in counteracting lipid peroxidation to inhibit ferroptosis and prove that this ancient pathway also acts as an important mechanism in p53-mediated tumor suppression. Notably, like FSP1,[20] VKORC1L1 is critical for catalyzing the reduced form of vitamin K to suppress ferroptosis. Most importantly, FSP1 and VKORC1L1 function independently, and both FSP1 and VKORC1L1 are required for the inhibitory effects on ferroptosis induced by vitamin K. Nevertheless, the difference between VKORC1L1 and FSP1 is also obvious. For example, vitamin K is the only substrate for VKORC1L1-mediated function in ferroptosis, whereas both CoQ_{10} and vitamin K (maybe even more) are the substrates of FSP1. While FSP1 is mainly localized at the plasma membrane (PM) to minimize the damage of lipid peroxides,[12,13] VKORC1L1 is predominantly an endoplasmic reticulum (ER) protein with four transmembrane domains.[26] Although further investigation is required, it is possible that FSP1 and VKORC1L1 function at different subcellular compartments to control the local levels of the lipid peroxidation occurring at PM and ER, respectively.

Vitamin K reduction in the canonical vitamin K cycle is mediated by VKORC1 and VKORC1L1, which provides the substrate for GGCX-mediated protein carboxylation. It is reported that *Vkorc1*- and *Ggcx*-knockout mice die shortly after birth, while *Vkorc1l1*-knockout mice can survive without adverse phenotypes. However, *Vkorc1l1/Vkorc1*-double-knockout mice lead to an earlier death than *Vkorc1*-knockout mice after birth, suggesting that *Vkorc1l1* participates but displays a non-essential role in vitamin K-dependent protein carboxylation.[23] On the contrary, we observed the limited activity of VKORC1 in regulating ferroptosis through promoting the reduced form of vitamin K. These differences indicate that the two vitamin K epoxide reductases have distinct roles that require further investigation. Our data indicate that *VKORC1L1* is a direct transcriptional target of p53 and that p53-mediated repression of *VKORC1L1* contributes at least in part to its tumor suppressive function. The data from the TCGA databases also support the oncogenic role of *VKORC1L1* in PAAD: *VKORC1L1* is overexpressed in tumor specimens, and high expression predicts poor survival outcomes. Patients with *VKORC1L1* genomic amplification also have significantly shorter overall survival. Consistent with our findings, *VKORC1L1* expression is strongly increased in the human cancer samples with mutated p53.

Limitations of the study
Our study indicates that VKORC1L1 is critical for ferroptosis by generating the reduced forms of vitamin K. VKORC1L1-mediated enzymatic activity on vitamin K was indeed validated by using the method developed by the Conrad lab. Due to the technical difficulty, no method is available to detect the levels of reduced forms of vitamin K directly *in vivo*. Future studies are required to further dissect the effects of VKORC1L1 on endogenous vitamin K hydroquinone levels, particularly during p53-mediated stress responses. Moreover, recently discovered anticoagulant drugs, DOACs and LMWHs, become the popular substitutes for warfarin. DOACs and LMWH directly inhibit thrombin activity without affecting VKOR enzymes (VKORC1L1 and VKORC1). Although DOACs and LMWHs are safer and more effective drugs that require less-frequent blood monitoring, recent studies point out that warfarin has much more pronounced survival advantages in pancreatic, gastric, and colorectal cancer patients than DOACs and LMWHs.[41,42] Indeed,

(B and C) Cell viability of PANC1 cells pretreated with warfarin (100 μM) for 24 h, then treated with RSL-3 (B) or TBH (C) for 8 h.

(D and E) Cell viability of AsPC1 cells pretreated with warfarin (100 μM) for 24 h, then treated with RSL-3 (D) or TBH (E) for 8 h.

(F) Tumor volume of AsPC1-derived tumors post oral administration with normal water, 1 mg/kg warfarin, or 2 mg/kg warfarin in *Nu/Nu* mice for indicated time.

(G) Xenograft tumors presentation of AsPC1-derived tumors post oral administration with normal water, 1 mg/kg warfarin, or 2 mg/kg warfarin in *Nu/Nu* mice. Scale bars, 1 cm.

(H) Tumor weights were determined from (G).

(I) Quantitative real-time PCR of *PTGS2* mRNA from tumors harvested from (G).

(J and K) Lipid peroxidation measurement (J) and ratio (K) of live cells derived from tumors from (G).

(L) Tumor volume of AsPC1-derived tumors post oral administration with normal water, 1 mg/kg warfarin, or combined 1 mg/kg warfarin and 1 mg/kg ferrostatin-1 in *Nu/Nu* mice for indicated time.

(M) Xenograft tumors presentation of AsPC1-derived tumors post oral administration with normal water, or 1 mg/kg warfarin, or combined 1 mg/kg warfarin and 1 mg/kg ferrostatin-1 in *Nu/Nu* mice. Scale bars, 1 cm.

(N) Tumor weights were determined from (M).

(O) Lipid peroxidation ratio of live cells derived from tumors from (M).

For (B)–(E), data are mean ± SD of n = 3, for (I) and (K), data are mean ± SD of n = 5, and for (O), data are mean ± SD of n = 6 independent biological repeats. For (F) and (H), data are mean ± SEM of n = 6, and for (L) and (N), data are mean ± SEM of n = 7 independent tumor samples. For (H) and (N), p values were calculated using one-way ANOVA. For (F), (I), (K), and (O), p values were calculated using unpaired, two-tailed Student's t test.

Cell Metabolism
Article

CellPress

our data demonstrate that warfarin is able to suppress tumor growth by promoting ferroptosis in both immunodeficient and immunocompetent tumor mouse models. Because warfarin and its derivatives have already been extensively used in the clinic, based on our findings, warfarin is a potential repurposing drug in cancer therapy, particularly for tumors with high levels of *VKORC1L1* expression. Finally, given the fact that VKORC1L1 and VKORC1 have differential roles in ferroptosis and that no obvious developmental abnormality is observed in *Vkorc1l1*-knockout mice,[23] new specific inhibitors for *VKORC1L1* should be developed, as they are likely more effective than warfarin in suppressing tumor growth through ferroptosis but without the potential bleeding risk or other toxicities in cancer therapy.

STAR★METHODS

Detailed methods are provided in the online version of this paper and include the following:

- KEY RESOURCES TABLE
- RESOURCE AVAILABILITY
  - Lead contact
  - Materials availability
  - Data and code availability
- EXPERIMENTAL MODEL AND STUDY PARTICIPANT DETAILS
  - Cell lines
  - Animals
- METHOD DETAILS
  - CRISPR screen and high-throughput sequencing
  - Analysis of CRISPR knockout library screen
  - CRISPR-Cas9 system mediated gene ablation
  - Plasmid generation and overexpression cell line generation
  - DPPH assay
  - Cystine starvation and glutamate treatment
  - Cell viability assay
  - Cell death staining
  - GSH/GSSG detection
  - Protein purification
  - Liposome preparation
  - *In vitro* STY-BODIPY autoxidation assay
  - Real-time quantitative PCR (RT-qPCR)
  - Chromatin Immunoprecipitation (ChIP)
  - Dual-luciferase Assay
  - Western blot
  - VKH_2 detection by chemical reduction
  - VKH_2 detection by *in vitro* activity assay
  - VKH_2 detection by LC-MS/MS
  - Vitamin K detection by ELISA assay
  - Lipid peroxidation analysis using C11-BODIPY
  - Mouse xenograft experiments
- QUANTIFICATION AND STATISTICAL ANALYSIS

SUPPLEMENTAL INFORMATION

Supplemental information can be found online at https://doi.org/10.1016/j.cmet.2023.06.014.

AUTHOR CONTRIBUTIONS

Conception and experimental design, X.Y., Z.W., and W.G.; CRISPR screen, X.Y., Z.W., Z.L., S.D., and Y.L.; cell experiments, X.Y. and Z.W; animal experiments, X.Y. and N.K.; LC-MS experiments, X.Y., Z.W., and F.Z.; manuscript writing – original draft, X.Y., Z.W., Y.L., and N.K.; manuscript writing – reviewing, X.Y., Z.W., F.Z., Z.Z., X.J., B.R.S., and W.G.; project supervision, W.G.

DECLARATION OF INTERESTS

B.R.S. is an inventor on patents and patent applications involving small-molecule drug discovery and ferroptosis; holds equity in Sonata Therapeutics; holds equity in and serves as a consultant to Exarta Therapeutics and ProJenX, Inc.; and serves as a consultant to Weatherwax Biotechnologies Corporation and Akin Gump Strauss Hauer & Feld LLP. X.J. is an inventor on patents related to autophagy and cell death and holds equity of and consults for Exarta Therapeutics and Lime Therapeutics.

INCLUSION AND DIVERSITY

We support inclusive, diverse, and equitable conduct of research.

REFERENCES

1. Dixon, S.J., Lemberg, K.M., Lamprecht, M.R., Skouta, R., Zaitsev, E.M., Gleason, C.E., Patel, D.N., Bauer, A.J., Cantley, A.M., Yang, W.S., et al. (2012). Ferroptosis: an iron-dependent form of nonapoptotic cell death. Cell *149*, 1060–1072. https://doi.org/10.1016/j.cell.2012.03.042.

2. Jiang, X., Stockwell, B.R., and Conrad, M. (2021). Ferroptosis: mechanisms, biology and role in disease. Nat. Rev. Mol. Cell Biol. *22*, 266–282. https://doi.org/10.1038/s41580-020-00324-8.

3. Doll, S., Proneth, B., Tyurina, Y.Y., Panzilius, E., Kobayashi, S., Ingold, I., Irmler, M., Beckers, J., Aichler, M., Walch, A., et al. (2017). ACSL4 dictates ferroptosis sensitivity by shaping cellular lipid composition. Nat. Chem. Biol. *13*, 91–98. https://doi.org/10.1038/nchembio.2239.

4. Kagan, V.E., Mao, G., Qu, F., Angeli, J.P.F., Doll, S., Croix, C.S., Dar, H.H., Liu, B., Tyurin, V.A., Ritov, V.B., et al. (2017). Oxidized arachidonic and adrenic PEs navigate cells to ferroptosis. Nat. Chem. Biol. *13*, 81–90. https://doi.org/10.1038/nchembio.2238.

5. Zou, Y., Henry, W.S., Ricq, E.L., Graham, E.T., Phadnis, V.V., Maretich, P., Paradkar, S., Boehnke, N., Deik, A.A., Reinhardt, F., et al. (2020). Plasticity of ether lipids promotes ferroptosis susceptibility and evasion. Nature *585*, 603–608. https://doi.org/10.1038/s41586-020-2732-8.

6. Yang, W.S., Kim, K.J., Gaschler, M.M., Patel, M., Shchepinov, M.S., and Stockwell, B.R. (2016). Peroxidation of polyunsaturated fatty acids by lipoxygenases drives ferroptosis. Proc. Natl. Acad. Sci. USA *113*. E4966–E4975. https://doi.org/10.1073/pnas.1603244113.

7. Chu, B., Kon, N., Chen, D., Li, T., Liu, T., Jiang, L., Song, S., Tavana, O., and Gu, W. (2019). ALOX12 is required for p53-mediated tumour

suppression through a distinct ferroptosis pathway. Nat. Cell Biol. *21*, 579–591. https://doi.org/10.1038/s41556-019-0305-6.

8. Jiang, L., Kon, N., Li, T., Wang, S.J., Su, T., Hibshoosh, H., Baer, R., and Gu, W. (2015). Ferroptosis as a p53-mediated activity during tumour suppression. Nature *520*, 57–62. https://doi.org/10.1038/nature14344.

9. Wenzel, S.E., Tyurina, Y.Y., Zhao, J., Croix, C.M.S., Dar, H.H., Mao, G., Tyurin, V.A., Anthonymuthu, T.S., Kapralov, A.A., Amoscato, A.A., et al. (2017). PEBP1 wardens ferroptosis by enabling lipoxygenase generation of lipid death signals. Cell *171*, 628–641.e26. https://doi.org/10.1016/j.cell.2017.09.044.

10. Song, S., Su, Z., Kon, N., Chu, B., Li, H., Jiang, X., Luo, J., Stockwell, B.R., and Gu, W. (2023). ALOX5-mediated ferroptosis acts as a distinct cell death pathway upon oxidative stress in Huntington's disease. Genes Dev. *37*, 204–217. https://doi.org/10.1101/gad.350211.122.

11. Yang, W.S., SriRamaratnam, R., Welsch, M.E., Shimada, K., Skouta, R., Viswanathan, V.S., Cheah, J.H., Clemons, P.A., Shamji, A.F., Clish, C.B., et al. (2014). Regulation of ferroptotic cancer cell death by GPX4. Cell *156*, 317–331. https://doi.org/10.1016/j.cell.2013.12.010.

12. Doll, S., Freitas, F.P., Shah, R., Aldrovandi, M., da Silva, M.C., Ingold, I., Goya Grocin, A., Xavier da Silva, T.N., Panzilius, E., Scheel, C.H., et al. (2019). FSP1 is a glutathione-independent ferroptosis suppressor. Nature *575*, 693–698. https://doi.org/10.1038/s41586-019-1707-0.

13. Bersuker, K., Hendricks, J.M., Li, Z., Magtanong, L., Ford, B., Tang, P.H., Roberts, M.A., Tong, B., Maimone, T.J., Zoncu, R., et al. (2019). The CoQ oxidoreductase FSP1 acts parallel to GPX4 to inhibit ferroptosis. Nature *575*, 688–692. https://doi.org/10.1038/s41586-019-1705-2.

14. Mao, C., Liu, X., Zhang, Y., Lei, G., Yan, Y., Lee, H., Koppula, P., Wu, S., Zhuang, L., Fang, B., et al. (2021). DHODH-mediated ferroptosis defence is a targetable vulnerability in cancer. Nature *593*, 586–590. https://doi.org/10.1038/s41586-021-03539-7.

15. Kraft, V.A., Bezjian, C.T., Pfeiffer, S., Ringelstetter, L., Müller, C., Zandkarimi, F., Merl-Pham, J., Bao, X., Anastasov, N., Kössl, J., et al. (2020). GTP cyclohydrolase 1/tetrahydrobiopterin counteract ferroptosis through lipid remodeling. ACS Cent. Sci. *6*, 41–53. https://doi.org/10.1021/acscentsci.9b01063.

16. Soula, M., Weber, R.A., Zilka, O., Alwaseem, H., La, K., Yen, F., Molina, H., Garcia-Bermudez, J., Pratt, D.A., and Birsoy, K. (2020). Metabolic determinants of cancer cell sensitivity to canonical ferroptosis inducers. Nat. Chem. Biol. *16*, 1351–1360. https://doi.org/10.1038/s41589-020-0613-y.

17. Sun, W.Y., Tyurin, V.A., Mikulska-Ruminska, K., Shrivastava, I.H., Anthonymuthu, T.S., Zhai, Y.J., Pan, M.H., Gong, H.B., Lu, D.H., Sun, J., et al. (2021). Phospholipase iPLA2β averts ferroptosis by eliminating a redox lipid death signal. Nat. Chem. Biol. *17*, 465–476. https://doi.org/10.1038/s41589-020-00734-x.

18. Chen, D., Chu, B., Yang, X., Liu, Z., Jin, Y., Kon, N., Rabadan, R., Jiang, X., Stockwell, B.R., and Gu, W. (2021). iPLA2β-mediated lipid detoxification controls p53-driven ferroptosis independent of GPX4. Nat. Commun. *12*, 3644. https://doi.org/10.1038/s41467-021-23902-6.

19. Kolbrink, B., von Samson-Himmelstjerna, F.A., Messtorff, M.L., Riebeling, T., Nische, R., Schmitz, J., Bräsen, J.H., Kunzendorf, U., and Krautwald, S. (2022). Vitamin K1 inhibits ferroptosis and counteracts a detrimental effect of phenprocoumon in experimental acute kidney injury. Cell. Mol. Life Sci. *79*, 387. https://doi.org/10.1007/s00018-022-04416-w.

20. Mishima, E., Ito, J., Wu, Z., Nakamura, T., Wahida, A., Doll, S., Tonnus, W., Nepachalovich, P., Eggenhofer, E., Aldrovandi, M., et al. (2022). A non-canonical vitamin K cycle is a potent ferroptosis suppressor. Nature *608*, 778–783. https://doi.org/10.1038/s41586-022-05022-3.

21. Li, W., Xu, H., Xiao, T., Cong, L., Love, M.I., Zhang, F., Irizarry, R.A., Liu, J.S., Brown, M., and Liu, X.S. (2014). MAGeCK enables robust identification of essential genes from genome-scale CRISPR/Cas9 knockout screens. Genome Biol. *15*, 554. https://doi.org/10.1186/s13059-014-0554-4.

22. Oldenburg, J., Marinova, M., Müller-Reible, C., and Watzka, M. (2008). The vitamin K cycle. Vitam. Horm. *78*, 35–62. https://doi.org/10.1016/S0083-6729(07)00003-9.

23. Lacombe, J., Rishavy, M.A., Berkner, K.L., and Ferron, M. (2018). VKOR paralog VKORC1L1 supports vitamin K–dependent protein carboxylation in vivo. JCI Insight *3*. https://doi.org/10.1172/jci.insight.96501.

24. Fukui, M., Song, J.H., Choi, J., Choi, H.J., and Zhu, B.T. (2009). Mechanism of glutamate-induced neurotoxicity in HT22 mouse hippocampal cells. Eur. J. Pharmacol. *617*, 1–11. https://doi.org/10.1016/j.ejphar.2009.06.059.

25. Cervellati, R., and Greco, E. (2016). In vitro antioxidant activity of ubiquinone and ubiquinol, compared to vitamin E. Helv. Chim. Acta *99*, 41–45. https://doi.org/10.1002/hlca.201500124.

26. Tie, J.K., Jin, D.Y., and Stafford, D.W. (2014). Conserved loop cysteines of vitamin K epoxide reductase complex subunit 1-like 1 (VKORC1L1) are involved in its active site regeneration. J. Biol. Chem. *289*, 9396–9407. https://doi.org/10.1074/jbc.M113.534446.

27. Shah, R., Farmer, L.A., Zilka, O., Van Kessel, A.T.M., and Pratt, D.A. (2019). Beyond DPPH: use of fluorescence-enabled inhibited autoxidation to predict oxidative cell death rescue. Cell Chem. Biol. *26*, 1594–1607.e7. https://doi.org/10.1016/j.chembiol.2019.09.007.

28. Zilka, O., Shah, R., Li, B., Friedmann Angeli, J.P., Griesser, M., Conrad, M., and Pratt, D.A. (2017). On the mechanism of cytoprotection by ferrostatin-1 and liproxstatin-1 and the role of lipid peroxidation in ferroptotic cell death. ACS Cent. Sci. *3*, 232–243. https://doi.org/10.1021/acscentsci.7b00028.

29. Chu, P.H., Huang, T.Y., Williams, J., and Stafford, D.W. (2006). Purified vitamin K epoxide reductase alone is sufficient for conversion of vitamin K epoxide to vitamin K and vitamin K to vitamin KH2. Proc. Natl. Acad. Sci. USA *103*, 19308–19313. https://doi.org/10.1073/pnas.0609401103.

30. Nakagawa, K., Sawada, N., Hirota, Y., Uchino, Y., Suhara, Y., Hasegawa, T., Amizuka, N., Okamoto, T., Tsugawa, N., Kamao, M., et al. (2014). Vitamin K2 biosynthetic enzyme, UBIAD1 is essential for embryonic development of mice. PLoS One *9*, e104078. https://doi.org/10.1371/journal.pone.0104078.

31. Göbel, A., Rauner, M., Hofbauer, L.C., and Rachner, T.D. (2020). Cholesterol and beyond - the role of the mevalonate pathway in cancer biology. Biochim. Biophys. Acta Rev. Cancer *1873*, 188351. https://doi.org/10.1016/j.bbcan.2020.188351.

32. Moon, S.H., Huang, C.H., Houlihan, S.L., Regunath, K., Freed-Pastor, W.A., Morris, J.P., 4th, Tschaharganeh, D.F., Kastenhuber, E.R., Barsotti, A.M., Culp-Hill, R., et al. (2019). p53 represses the mevalonate pathway to mediate tumor suppression. Cell *176*, 564–580.e19. https://doi.org/10.1016/j.cell.2018.11.011.

33. Kavanagh, K.L., Guo, K., Dunford, J.E., Wu, X., Knapp, S., Ebetino, F.H., Rogers, M.J., Russell, R.G.G., and Oppermann, U. (2006). The molecular mechanism of nitrogen-containing bisphosphonates as antiosteoporosis drugs. Proc. Natl. Acad. Sci. USA *103*, 7829–7834. https://doi.org/10.1073/pnas.0601643103.

34. Kirschner, K., Samarajiwa, S.A., Cairns, J.M., Menon, S., Pérez-Mancera, P.A., Tomimatsu, K., Bermejo-Rodriguez, C., Ito, Y., Chandra, T., Narita, M., et al. (2015). Phenotype specific analyses reveal distinct regulatory mechanism for chronically activated p53. PLoS Genet. *11*, e1005053. https://doi.org/10.1371/journal.pgen.1005053.

35. Younger, S.T., Kenzelmann-Broz, D., Jung, H., Attardi, L.D., and Rinn, J.L. (2015). Integrative genomic analysis reveals widespread enhancer regulation by p53 in response to DNA damage. Nucleic Acids Res. *43*, 4447–4462. https://doi.org/10.1093/nar/gkv284.

36. Abbas, T., and Dutta, A. (2009). p21 in cancer: intricate networks and multiple activities. Nat. Rev. Cancer *9*, 400–414. https://doi.org/10.1038/nrc2657.

37. Hermeking, H. (2012). MicroRNAs in the p53 network: micromanagement of tumour suppression. Nat. Rev. Cancer *12*, 613–626. https://doi.org/10.1038/nrc3318.

38. Goldman, M.J., Craft, B., Hastie, M., Repečka, K., McDade, F., Kamath, A., Banerjee, A., Luo, Y., Rogers, D., Brooks, A.N., et al. (2020). Visualizing and interpreting cancer genomics data via the Xena platform. Nat. Biotechnol. *38*, 675–678. https://doi.org/10.1038/s41587-020-0546-8.

Cell Metabolism
Article

39. Hammed, A., Matagrin, B., Spohn, G., Prouillac, C., Benoit, E., and Lattard, V. (2013). VKORC1L1, an enzyme rescuing the vitamin K 2,3-epoxide reductase activity in some extrahepatic tissues during anticoagulation therapy. J. Biol. Chem. *288*, 28733–28742. https://doi.org/10.1074/jbc.M113.457119.

40. Westhofen, P., Watzka, M., Marinova, M., Hass, M., Kirfel, G., Müller, J., Bevans, C.G., Müller, C.R., and Oldenburg, J. (2011). Human vitamin K 2,3-epoxide reductase complex subunit 1-like 1 (VKORC1L1) mediates vitamin K-dependent intracellular antioxidant function. J. Biol. Chem. *286*, 15085–15094. https://doi.org/10.1074/jbc.M110.210971.

41. Chiasakul, T., Redd, R., Patell, R., Khan, A.M., McCarthy, E.P., Neuberg, D., and Zwicker, J.I. (2021). Overall survival with warfarin vs. low-molecular-weight heparin in cancer-associated thrombosis. J. Thromb. Haemost. *19*, 2825–2834. https://doi.org/10.1111/jth.15519.

42. Chiasakul, T., and Zwicker, J.I. (2022). The impact of warfarin on overall survival in cancer patients. Thromb. Res. *213* (Suppl 1). S113–S119. https://doi.org/10.1016/j.thromres.2021.11.004.

43. Tang, Z., Kang, B., Li, C., Chen, T., and Zhang, Z. (2019). GEPIA2: an enhanced web server for large-scale expression profiling and interactive analysis. Nucleic Acids Res. *47*. W556–W560. https://doi.org/10.1093/nar/gkz430.

44. Badgley, M.A., Kremer, D.M., Maurer, H.C., DelGiorno, K.E., Lee, H.J., Purohit, V., Sagalovskiy, I.R., Ma, A., Kapilian, J., Firl, C.E.M., et al. (2020). Cysteine depletion induces pancreatic tumor ferroptosis in mice. Science *368*, 85–89. https://doi.org/10.1126/science.aaw9872.

45. Li, J., Byrne, K.T., Yan, F., Yamazoe, T., Chen, Z., Baslan, T., Richman, L.P., Lin, J.H., Sun, Y.H., Rech, A.J., et al. (2018). Tumor cell-intrinsic factors underlie heterogeneity of immune cell infiltration and response to immunotherapy. Immunity *49*, 178–193.e7. https://doi.org/10.1016/j.immuni.2018.06.006.

46. Concordet, J.P., and Haeussler, M. (2018). CRISPOR: intuitive guide selection for CRISPR/Cas9 genome editing experiments and screens. Nucleic Acids Res. *46*. W242–W245. https://doi.org/10.1093/nar/gky354.

47. Birsoy, K., Wang, T., Chen, W.W., Freinkman, E., Abu-Remaileh, M., and Sabatini, D.M. (2015). An essential role of the mitochondrial electron transport chain in cell proliferation is to enable aspartate synthesis. Cell *162*, 540–551. https://doi.org/10.1016/j.cell.2015.07.016.

48. Liu, J., Lichtenberg, T., Hoadley, K.A., Poisson, L.M., Lazar, A.J., Cherniack, A.D., Kovatich, A.J., Benz, C.C., Levine, D.A., Lee, A.V., et al. (2018). An integrated TCGA pan-cancer clinical data resource to drive high-quality survival outcome analytics. Cell *173*, 400–416.e11. https://doi.org/10.1016/j.cell.2018.02.052.

STAR★METHODS

KEY RESOURCES TABLE

REAGENT or RESOURCE	SOURCE	IDENTIFIER
Antibodies		
Anti-VKORC1L1	Atlas Antibodies	Cat# HPA053954; RRID: AB_2682319
Anti-VKORC1	Atlas Antibodies	Cat# HPA042720; RRID: AB_10961864
Anti-Actin	Sigma-Aldrich	Cat# A3853; RRID: AB_262137
Anti-Vinculin	Sigma-Aldrich	Cat# V9131; RRID: AB_477629
Anti-Flag	Sigma-Aldrich	Cat# F-3165; RRID: AB_259529
Anti-p53 (CM5)	Leica Biosystems	Cat#NCL-L-p53-CM5p; RRID: AB_2895247
Anti-p53 (DO-1)	Santa Cruz Biotechnology	Cat# sc-126; RRID: AB_628082
Anti-ACSL4	Santa Cruz Biotechnology	Cat# sc-271800; RRID: AB_10715092
Anti-MDM2	Santa Cruz Biotechnology	Cat# sc-965; RRID: AB_627920
Anti-FSP1(AMID)	Santa Cruz Biotechnology	Cat# sc-377120; RRID: AB_2893240
Anti-ACSL3	Santa Cruz Biotechnology	Cat# sc-166374; RRID: AB_2222425
Anti-p21	Cell Signaling Technology	Cat# 2947; RRID: AB_823586
Anti-xCT/SLC7A11	Cell Signaling Technology	Cat#12691S; RRID: AB_2687474
Anti-GPX4	Abcam	Cat# ab125066; RRID: AB_10973901
Anti-GGCX	ABclonal	Cat# A1806; RRID: AB_2763845
Anti-FDPS	Proteintech	Cat# 16129-1-AP; RRID: AB_2104749
Anti-DGCR8	Bethyl Laboratories	Cat# A302-468A; RRID: AB_1944223
Anti-UBIAD1	Novus Biologicals	Cat# NBP2-93542
Bacterial and virus strains		
DH5α Competent Cells	ThermoFisher	18265017
TOP10 Competent Cells	ThermoFisher	C404006
ElectroMAX Stbl4 Competent Cells	ThermoFisher	11635018
Chemicals, peptides, and recombinant proteins		
Tert-butyl hydroperoxide (TBH)	Sigma-Aldrich	458139; CAS: 75-91-2
Imidazole ketone erastin (IKE)	MedChemExpress	HY-114481; CAS:1801530-11-9
1S,3R-RSL-3	Sigma-Aldrich	SML2234; CAS:1219810-16-8
N-acetyl-L-cysteine (NAC)	Sigma-Aldrich	A7250; CAS: 616-91-1
Ferrostatin-1 (Ferr-1)	Sigma-Aldrich	SML0583; CAS: 347174-05-4
Liproxstatin-1 (Lipro-1)	Sigma-Aldrich	SML1414; CAS: 950455-15-9
Deferoxamine (DFO)	Sigma-Aldrich	D9533; CAS: 138-14-7
Vitamin K1, phylloquinone	Sigma-Aldrich	V3501; CAS: 84-80-0
Vitamin K2, menaquinone	Sigma-Aldrich	V9378; CAS: 863-61-6
α-Tocopherol (vitamin E)	Sigma-Aldrich	T3251; CAS: 10191-41-0
α-Ascorbic acid (vitamin C)	Sigma-Aldrich	A92902; CAS: 50-81-7
Farnesyl pyrophosphate ammonium salt (FPP)	Sigma-Aldrich	F6892; CAS: 13058-04-3
Warfarin	Sigma-Aldrich	A2250; CAS: 81-81-2
Doxorubicin hydrochloride (Doxo)	Sigma-Aldrich	D1515; CAS: 25316-40-9
Nutlin-3	Sigma-Aldrich	N6287; CAS: 548472-68-0
L-α-Phosphatidylcholine	Sigma-Aldrich	P3556; CAS: 8002-43-5
2,2′-Azobis(2-methylpropionamidine) dihydrochloride (AAPH)	Sigma-Aldrich	440914; CAS: 2997-92-4
Sodium borohydride	Sigma-Aldrich	213462; CAS: 16940-66-2
2,2-Diphenyl-1-picrylhydrazyl (DPPH)	Sigma-Aldrich	D9132; CAS: 1898-66-4
BODIPY 581/591 C11 dye	ThermoFisher	D3861; CAS: 217075-36-0

(Continued on next page)

Cell Metabolism
Article

🔗 **CellPress**

Continued

REAGENT or RESOURCE	SOURCE	IDENTIFIER
STY-BODIPY probes	Cayman	27089; CAS: 2383063-37-2
SYTOX green dead cell stain	ThermoFisher	S34860; CAS: 2383063-37-2
Anti-Flag agarose beads	Sigma-Aldrich	A2220
Flag-peptide	Sigma-Aldrich	F3290
Lipofectamine 3000	ThermoFisher	L3000150
Lipofectamine CRISPRMAX Cas9	ThermoFisher	CMAX00015
TrueCut Cas9 Protein v2	ThermoFisher	A36498
Critical commercial assays		
CellTiter-Glo 2.0 Cell Viability Assay	Promega	G9243
GSH/GSSG-Glo Assay	Promega	V6611
Dual-Luciferase Reporter Assay System	Promega	E1910
Human vitamin K ELISA Kit	MyBioSource	MBS746981
Deposited data		
Raw data	This paper	Mendeley data http://doi.org/10.17632/8mxhzbr3v3.1
Experimental models: Cell lines		
Human: HEK293T	ATCC	CRL-3216
Human: A375	ATCC	CRL-1619
Human: NCI-H1299	ATCC	CRL-5803
Human: HT1080	ATCC	CCL-121
Human: U2OS	ATCC	HTB-96
Human: PANC1	Kenneth Olive	N/A
Human: AsPC1	Kenneth Olive	N/A
Human: BxPC3	Kenneth Olive	N/A
Human: MIAPaCa2	Kenneth Olive	N/A
Human: S2-013	Kenneth Olive	N/A
Mouse HT-22	Sigma-Aldrich	SCC129
Mouse Embryonic Fibroblasts, MEFs	This paper	N/A
KrasLSL-G12D/+; Trp53LSL-R172H/+; Pdx1-Cre; Rosa26YFP/YFP Mouse Pancreatic Cancer Cell Line (7160c2)	Kerafast	EUP008-FP; Li et al.[45]
A375 VKORC1 KO	This paper	N/A
A375 GGCX KO	This paper	N/A
A375 VKORC1L1 KO	This paper	N/A
A375 VKORC1L1/VKORC1 DKO	This paper	N/A
HT1080 VKORC1L1 KO	This paper	N/A
A375 GPX4 KO	This paper	N/A
A375 GPX4/VKORC1L1 DKO	This paper	N/A
A375 FDPS KO	This paper	N/A
A375 FSP1 KO	This paper	N/A
A375 FSP1/VKORC1L1 DKO	This paper	N/A
HCT116 p21/DGCR8 DKO	This paper	N/A
A375 p53 KO	This paper	N/A
U2OS p53 KO	This paper	N/A
A375 VKORC1L1 KO + VKORC1	This paper	N/A
A375 + UBIAD1	This paper	N/A
A375 VKORC1L1 KO + UBIAD1	This paper	N/A
A375 + VKORC1L1	This paper	N/A
A375 p53 KO + VKORC1L1	This paper	N/A

Continued

REAGENT or RESOURCE	SOURCE	IDENTIFIER
Experimental models: Organisms/strains		
C57BL/6 mouse	Charles River	000664
NU/NU nude mouse	Charles River	088
Oligonucleotides		
Negative Control non-targeting sgRNA	ThermoFisher	A35526
VKORC1L1 sgRNA #1	ThermoFisher	CRISPR910373_SGM
VKORC1L1 sgRNA #2	ThermoFisher	CRISPR829919_SGM
GPX4 sgRNA	ThermoFisher	CRISPR662855_SGM
FDPS sgRNA #1	ThermoFisher	CRISPR631102_SGM
FDPS sgRNA #2	ThermoFisher	CRISPR631105_SGM
p21 sgRNA	ThermoFisher	CRISPR865085_SGM
DGCR8 sgRNA	ThermoFisher	CRISPR730402_SGM
VKORC1 sgRNA #1: 5' - GACGCGCGAACAGCTGATGG -3'	Synthego	N/A
VKORC1 sgRNA #2: 5' - GCGAGAGCACTAAGCCCGTC -3'	Synthego	N/A
GGCX sgRNA #1: 5' - CCTGCACGATGTCCACACGA -3'	Synthego	N/A
GGCX sgRNA #2: 5' - GACCCTGCTGAATCGACCAA -3'	Synthego	N/A
FSP1 sgRNA: 5' - TCCCGATTCCACCGAGACCT -3'	Synthego	N/A
Primers used for RT-qPCR were listed in Table S1	Sigma-Aldrich	N/A
Primers used for ChIP-qPCR were listed in Table S2	Sigma-Aldrich	N/A
Recombinant DNA		
pLVX-M-puro-Flag-VKORC1L1	This paper	N/A
pLVX-M-puro-Flag-VKORC1L1-C50S	This paper	N/A
pLVX-M-puro-Flag-VKORC1L1-C58S	This paper	N/A
pLVX-M-puro-VKORC1	This paper	N/A
pLVX-M-puro-Flag-UBIAD1	This paper	N/A
pGL3-Basic-VKORC1L1-RE	This paper	N/A
pGL3-Basic-VKORC1L1-mutRE	This paper	N/A
pCIN4-p53	This paper	N/A
pCIN4-Flag-p53 WT	This paper	N/A
pCIN4-Flag-HA-p53 R175H	This paper	N/A
pCIN4-Flag-p53 R248W	This paper	N/A
pCIN4-Flag-p53 R273H	This paper	N/A
Software and algorithms		
FlowJo v10	BD Biosciences	https://www.flowjo.com/
GraphPad Prism 8.0	GraphPad Software	https://www.graphpad.com/
ImageJ	NIH	https://imagej.nih.gov/ij/
CRISPOR	Concordet and Haeussler[46]	http://crispor.tefor.net/crispor.py
MAGeCK	Li et al.[21]	https://github.com/liulab-dfci/MAGeCK
UCSC Xena Platform	Goldman et al.[38]	https://xenabrowser.net/
R (v 4.0.5)	R project	http://r-project.org/
GEPIA2 web server	Tang et al.[43]	http://gepia2.cancer-pku.cn/#analysis
Other		
Liu human CRISPR knockout library	Addgene	1000000132
Human CRISPR metabolic gene knockout library	Addgene	110066
Publicly available data (p53 ChIP-seq in IMR90)	Kirschner et al.[34]	GEO: GSE53491
Publicly available data (p53 ChIP-seq in MEFs)	Younger et al.[35]	GEO: GSE55727

Cell Metabolism
Article

CellPress

RESOURCE AVAILABILITY

Lead contact

Further information and requests for resources and reagents should be directed to and will be fulfilled by the lead contact, Wei Gu (wg8@cumc.columbia.edu).

Materials availability

All the materials generated in this study (see key resources table) are available upon request from the lead contact. This study did not generate unique reagents.

Data and code availability

- All data reported in this study are available from the lead contact upon request. Uncropped Western blots and all raw data used to generate graphs are uploaded in Mendeley data (http://doi.org/10.17632/8mxhzbr3v3.1).
- This paper does not report the original codes.
- Any additional information required to reanalyze the data reported in this paper is available from the lead contact upon request.

EXPERIMENTAL MODEL AND STUDY PARTICIPANT DETAILS

Cell lines

Human embryonic kidney HEK293T, human fibrosarcoma HT1080 (p53 wildtype), human bone osteosarcoma U2OS (p53 wildtype), human melanoma A375 (p53 wildtype), and human non-small cell lung carcinoma H1299 (p53-null) were previously obtained from American Type Culture Collection (ATCC). Mouse hippocampal HT22 cells were previously obtained from Sigma-Aldrich. Human pancreatic cancer PANC1, AsPC1, BxPC3, MIAPaCa2, and S2-013 cells were kind gifts from Kenneth Olive Lab (Columbia University). Cells were cultured with DMEM containing 10% (v/v) fetal bovine serum (FBS) (Gibco), 100 units/mL penicillin, and 100 μg/mL streptomycin (Gibco). KPCY cells were contributed by Ben Z. Stanger lab.[45] KPCY cells were cultured with DMEM (high glucose without sodium pyruvate) containing 10% (v/v) FBS, 2mM glutamine (Invitrogen), 100 units/mL penicillin, and 100 μg/mL streptomycin. MEFs were generated from day 13.5 embryos according to standard procedures. MEFs were cultured with DMEM containing 10% (v/v) heat inactivated FBS and 1% non-essential amino acids (Gibco), 100 units/mL penicillin, and 100 μg/mL streptomycin. Cells were cultured in a 10cm plate and seeded into 6-well plates, 12-well plates, or 96-well plates for cell viability and lipid peroxidation analysis. All cell lines were incubated at 37 °C with a humidified atmosphere of 5% CO_2. All cell lines have been regularly tested to be negative for mycoplasma contamination every month. No cell lines used in this work were listed in the ICLAC database.

Animals

All the mice were housed in a temperature-controlled room (65–75 °F) with 40–60% humidity, with a light/dark cycle of 12 hours/12 hours. All animal experiments were approved by the Institutional Animal Care and Use Committee (IACUC) at Columbia University under the supervision of the Institute of Comparative Medicine (ICM).

Six weeks old female nude mice (*Nu/Nu*, Charles River) were used for establishing immunodeficient xenograft mouse model. Eight weeks old female mice (C57BL/6,Charles River) were used for establishing immunocompetent xenograft mouse model. Randomization of animals was performed before the xenograft experiments. The tumors in the xenograft experiments did not exceed the limit for tumor burden (10% of total body weight or 2 cm in diameter).

METHOD DETAILS

CRISPR screen and high-throughput sequencing

For the genome wide CRISPR knockout screen, Liu human CRISPR knockout library (H1 and H2) was received as a gift from Xiaole Shirley Liu. H2 library contains a total of 92871 sgRNAs for 18436 gene targets with 5 sgRNAs per gene. Library amplification, lentiviral packaging, and titration were all done according to the standard protocol. For transduction, 1.25×10^8 A375 cells (around 400× coverage) were infected with the H2 library at a multiplicity of infection (MOI) of around 0.3. 48h after transduction, T_0 cells were harvested. The rest cells were selected with 0.9 μg/mL puromycin for 48h, and 5×10^7 cells were passed every 48–72h for 14 days. Then, T_{14} cells were harvested. 1×10^8 cells were treated with DMSO or 0.75μM RSL-3 for 5 days.

For the metabolic gene CRISPR knockout screen, the human CRISPR metabolic gene knockout library was received as a gift from David Sabatini.[47] The library contains a total of 30290 sgRNAs for 2981 gene targets with 10 sgRNAs per gene. Library amplification, lentiviral packaging, and titration were all done according to the standard protocol. For transduction, 1.25×10^8 A375 cells (around 1,000×coverage) were infected with the metabolic library at a multiplicity of infection (MOI) of around 0.3. 48h after transduction, T_0 cells were harvested. The rest cells were selected with 0.9 μg/mL puromycin for 48h, and 4×10^7 cells were passaged every 48–72h for 14 days. Then, T_{14} cells were harvested. 1×10^8 cells were treated with DMSO or 5μM IKE for 7 days.

After indicated treatment, live cells were collected, and genomic DNA was isolated using the Wizard Genomic DNA Purification Kit (Promega, A1120). The high-throughput sequencing libraries were prepared through two-step PCR amplification. For the first step, 2.5 μg of genomic DNA was used in a 50 μL per PCR reaction of a total 96 reaction by Phusion Plus DNA Polymerase (ThermoFisher, F630XL). PCR primers pairs for first PCR: Shared Forward P5 by two screens, 5'- TCGTCGGCAGCGTCAGATGTGTATAAG AGACAGTTGTGGAAAGGACGAAACACCG -3'; Reverse P7 for genome wide gene CRISPR knockout screen 5'- GTCTCGTG GGCTCGGAGATGTGTATAAGAGACAGCCAATTCCCACTCCTTTCAAGACCT -3'; Reverse P7 for metabolic gene CRISPR knockout screen 5'-GTCTCGTGGGCTCGGAGATGTGTATAAGAGACAGTCTACTATTCTTTCCCCTGCACTGT-3'. For the second step, PCR amplification was done for adding the specific barcode. High throughput sequencing was done by using the Illumina HiSeq2500.

Analysis of CRISPR knockout library screen
MAGeCK software was used for CRISPR-Cas9 screen analysis. Briefly, the resulting sequencing data were debarcoded, merged, and then the 43 bp single-end reads contained 20-bp sgRNA sequence was aligned to the reference sgRNA library of CRISPR knockout library using 'count' function from MAGeCK without allowing for any mismatches. MAGeCK built a linear model to estimate the variance of guide RNA read counts and evaluated the guide RNA abundance changes between control and treatment conditions. MAGeCK provides a new subcommand, mle algorithm, to calculate gene essentiality from CRISPR screens. MAGeCK-mle was used to detect P value and beta score for positive and negative selection under the method normalizing to the median counts of sgRNAs. The Beta (β) score is similar with the term guide-level log_2 fold change, where a positive beta score means a gene is positively selected, and a negative beta score means a gene is negatively selected.

CRISPR-Cas9 system mediated gene ablation
p53 knockout cells were previously describe.[18] To generate indicated knockout cell line in A375, HT1080, or HCT116, gene synthetic guide RNA (sgRNAs) or Negative Control non-targeting RNA was co-transfected with TrueCut Cas9 protein v2 by Lipofectamine CRISPRMAX Transfection Reagent according to reagent instructions. Parts of cells transfected with sgRNA were harvested for western blot analysis to validate the efficiency of sgRNA. And the rest of the cells were split into single cells to produce single colonies during around two to four weeks culture. Further, western blot was applied to identify indicated knockout cells. VKORC1 and GGCX sgRNAs were designed by CRISPOR[46] and synthesized by Synthego. Other sgRNAs were purchased from Invitrogen. The sgRNA sequence or sgRNA catalog number purchased from Invitrogen were shown in key resources table.

Plasmid generation and overexpression cell line generation
Human VKORC1L1 open reading frame clone was purchased from ORIGENE (RC205726) and then sub-cloned into pLVX-M-puro (Addgene, plasmid #125839). VKORC1L1 C50S or C58S mutant plasmids were constructed by using Phusion High-Fidelity DNA Polymerase (Thermo Fisher, F530L) according to the manufacture' protocol. UBIAD1 and VKORC1 cDNA were amplified from HCT116 cDNA reversed by SuperScript IV VILO Master Mix (Invitrogen) and sub-cloned into pLVX-M-puro vector. VKORC1L1, VKORC1L1 C50S, VKORC1L1 C58S, UBIAD1, or VKORC1 pLVX plasmids were co-transfected with viral packaging plasmids (psPAX2 and pMD2G) into HEK293T cells according to the ratio of plasmids is 4:3:1 using Lipofectamine 3000 Reagent. After 48 hours transfections, medium of HEK293T cells was collected and filtered with 0.45μm PES filter. Further, A375 or HT1080 cells were infected with vital medium for 12 hours and split into single cells. Cells were selected with 1 μg/mL puromycin for 2 weeks and performed western blot analysis to identify protein overexpressing level.

DPPH assay
2,2-diphenyl-1-picrylhydrazyl (DPPH) were prepared in 50μM solution with methanol. And 1μl indicated compound in DMSO were added into 1mL prepared DPPH buffer and rotated for 10 minutes at room temperature. Every group was set for triplicate. 1mL reaction were measured at an absorbance of 517nm with Ultrospec 2100 Pro UV/Spectrometer (Amersham Biosciences). Methanol was used as blank.

Cystine starvation and glutamate treatment
For cystine starvation, cells were trypsinized and washed with PBS three times. Then, cells were seeded into cystine-deficient DMEM (Invitrogen, 21013024) supplemented with 4 mM glutamine (Sigma-Aldrich, G8540) and 200 μM methionine (Sigma-Aldrich, M5308) containing 10% FBS in presence indicated concentration of cystine (Sigma-Aldrich, C7602).

For glutamate treatment, HT22 cells were sub-cultured into regular DMEM medium with or without 4mM glutamate (Sigma-Aldrich, G1251) for 16 hours and cell viability tests were further performed.

Cell viability assay
Without specific mention, 5×10^3 per well indicated cells were seeded into a 96-well microplate (PerkinElmer) overnight. Cystine starvation, glutamate treatment, or ferrostatin-1 withdrawal were applied to cells during seeding on 96-well plates with indicated chemicals for indicated time. For overnight adhered cells, cells were treated with RSL-3, TBH, or IKE for indicated time, accompanied by adding indicated chemicals. Warfarin or Nutlin-3 pre-treatment was performed after cells adhered. For evaluating the protective effects of vitamin K in VKORC1L1/GPX4 double knockout cells, 2×10^3 per well cells which were withdrawn ferrostatin-1 were seeded into a 96-well microplate by treating with vitamin K for 72h.

Cell Metabolism
Article

🔗 **CellPress**

There were three biological replicates per experiment condition. Before testing cell viability, 96-well plate stood still at room temperature for 30 minutes. And cellular ATP levels were measured with CellTiter-Glo 2.0 Cell Viability Assay reagent following the manufacturer's instructions. Then, the plates were immediately transferred to GloMax Discover Microplate Reader (Promega). Cell viability was calculated by ATP level of treated group compared to untreated group. 100 percentage of cell viability was regarded as 0 percentage of cell death. Nonlinear regression analysis was used to measure the fit curves of cell viability and calculate the IC50/EC50 value by GraphPad Prism 8.0.

Cell death staining
4×10^4 cells were seeded in 12-well plate per well one day prior to the experiment. After indicated treatment, medium was replaced with fresh medium containing 30 nM SYTOX green dead cell stain and incubated for 1h at 37°C. Three images per experiment condition were captured with both Bright channel and green channel by microscopy (Olympus, IX51).

GSH/GSSG detection
Cells were treated under indicated conditions for indicated time by adding indicated chemical. GSH/GSSG ratio was measured by following the manufacturer's instructions of GSH/GSSG-Glo Assay.

Protein purification
Flag tagged VKORC1L1 wildtype, C50S mutant or C58S mutant expressing plasmids were transfected in HEK293T cells with Lipofectamine 3000 transfection reagent. Cells were harvested after 48 hours transfection and sonicated in BC500 buffer (50 mM Tris-HCl pH 7.3, 500 mM NaCl, 0.1 mM EDTA, 0.4% NP-40, and 10% glycerol) for 5 minutes. Cell lysate was added with corresponding amount of M2 Affinity Gel and incubated overnight at 4 °C. Next day, protein-binding beads were washed with BC500 buffer six times and then eluted with Flag peptide four times at 4°C. The elution was concentrated with 10kDa Amicon Ultra-0.5 Centrifugal Filter Unit (Sigma-Aldrich, UFC501024). Concentrated protein was quantified with SDS-PAGE gel and stained by GelCode Blue Stain Reagent (ThermoFisher, 24592). Bovine serum albumin proteins (BSA) were applied for normalization.

Liposome preparation
Chloroform solved egg PC were mixed in a dry vial and then evaporated under vacuum to yield a thin film on the vial wall. The lipid film was then resuspended in PBS, yielding a 20mM lipid suspension. The lipid suspension was subjected to 3 times of 2 minutes dry ice freezing, 5 minutes room temperature thawing, and 1minutes sonication cycles. The lipid suspension was then extruded 25 times using a mini extruder (Avanti Polar Lipids, 610000) equipped with a 100 nm polycarbonate membrane to form homogeneous liposomes.

In vitro STY-BODIPY autoxidation assay
1mM Egg PC liposomes, 1μM STY-BODIPY probes, 500μM DTT and indicated concentration of vitamin K were pre-mixed together for 5 minutes at 37°C in a Black 96-well Microplate (PerkinElmer, 6005320) in PBS (pH 7.4) before adding indicated concentration of recombinant VKORC1L1 proteins. After this, VKORC1L1 proteins were added to the reaction system. Then, the autoxidation was initiated by adding 1mM 2,2′-Azobis(2-methylpropionamidine) dihydrochloride (AAPH) followed by vigorously mixing for 30 seconds. The data was acquired by the fluorescence signals of excitation 488 nm and emission 518 nm every minute for 180 to 200 minutes.

Real-time quantitative PCR (RT-qPCR)
Total RNA of A375, HCT116, U2OS, MEFs cells or tumor tissues was isolated using TRIzol reagent (Invitrogen) according to the manufacturer's instructions. Reverse transcription of template RNA into cDNA was conducted by SuperScript IV VILO Master Mix (Invitrogen). qPCR was performed with SYBR Green Master Mix (Invitrogen) to detect the target genes mRNA expression levels. All samples were run in triplicate. *GAPDH* or *Actin* expression level was used for normalization. The RT-qPCR primers were listed in Table S1.

Chromatin Immunoprecipitation (ChIP)
A375, HCT116 or MEFs cells were treated with 0.4 μg/mL doxorubicin for 24 hours and fixed with 1% formaldehyde for 15 minutes. Medium was added 0.125 M glycine for 10 minutes incubation to stop fixing. Then, cells were harvested and lysed with ChIP lysis buffer (10 mM Tris-HCl pH 8.0, 5 mM EDTA,150 mM NaCl, and 0.5% NP-40) containing protease inhibitor cocktail for 10 minutes on ice. After that, cell pellet was collected and sonicated with RIPA lysis buffer (10 mM Tris-HCl pH 8.0, 5 mM EDTA,150 mM NaCl, 0.1% SDS, 1% Triton X-100, and 0.5% DOC) containing protease inhibitor cocktail. The cell lysate was pre-cleaned with Protein A salmon sperm DNA agarose (Millipore, 16-157) for 2 hours at 4°C. Equal protein amount of cell lysate was incubated with 2μg p53 (DO-1) antibody applied in A375 and HCT116 cells, p53 (CM5) antibody applied in MEFs cells, 2 μg corresponded mouse or rabbit IgG control overnight at 4°C. Next day, 20 μl Protein A salmon sperm DNA agarose was coupled with antibody for 4 hours at 4 °C. and then rinsed with RIPA lysis buffer, High Salt Wash buffer (20 mM Tris-HCl pH 8.0, 500 mM NaCl, 5 mM EDTA, 0.1% SDS, 1% Triton X-100), LiCl Wash Buffer (10 mM Tris-HCl pH 8.0, 1 mM EDTA, 250 mM LiCl, 1% DOC, 1% NP-40), and TE buffer (10 mM Tris-HCl pH 8.0, 1 mM EDTA) for once, respectively. Coupled DNA-protein complex was eluted in Elution buffer (1% SDS and 100 mM NaHCO₃) twice and cross-linking was reversed at 65 °C overnight incubation. Next day, the complex was incubated with

Proteinase K for 1 hour and the binding DNA was extracted according to QIquick PCR Purification Kit (QIAGEN, 28104) protocol. ChIP samples were quantified by qPCR. DNA immunoprecipitated by IgG control was served as a negative control. The ChIP-qPCR primers were listed in Table S2.

Dual-luciferase Assay
VKORC1L1 genomic region from TSS +315 to +714 was sub-cloned into pGL3-Basic plasmid (E1751, Promega). Briefly, in 12-well plate, the reporter plasmids and *Renilla* control reporter plasmids were co-transfected into H1299 cells for 24 hours and the relative luciferase activity was measured according to the manufacturer's protocol of Dual-Luciferase Reporter Assay System by GloMax Discover Microplate Reader.

Western blot
Indicated cells were lysed in Flag lysis buffer [50 mM Tris-HCl (pH 7.9), 137 mM NaCl, 1% Triton X-100, 0.2% Sarkosyl, 1 mM NaF, 1 mM Na_3VO_4, and 10% glycerol] containing protease inhibitor cocktail and 1 mM dithiothreitol, and 1 mM phenylmethyl sulfonyl fluoride. Cell lysis was centrifuged, and the supernatant was collected. Protein samples were quantified with Bio-Rad Protein Assay Dye Reagent (Bio-Rad, 5000006). The same amount of protein from different experiment groups was examined with western blot analysis. Western blot was conducted for protein analysis according to standard methods with 4%-20% pre-cast SDS–PAGE gel (Invitrogen, XP0420). Commercial antibodies were shown in key resources table. Horseradish peroxidase-conjugated goat anti-mouse and anti-rabbit secondary antibody (Jackson ImmunoResearch) were visualized by ECL (Thermo Fisher, 32106) or SuperSignal (Thermo Fisher, 34076).

VKH_2 detection by chemical reduction
VKH_2 chemical reduction by MK4 was measured, as described.[20] Briefly, 1 mg $NaBH_4$ (sodium borohydride) was added to 200 μL of 1mM MK4 (dissolved in chloroform: methanol; 1:19 v/v) and incubated on ice for 1 minute. After the reaction, 10 μL of reaction solvent was quickly diluted by 490 μL pre-chilled methanol and then analyzed by LC–MS/MS.

VKH_2 detection by *in vitro* activity assay
VKH_2 level by *in vitro* activity assay detected as described previously.[20] Briefly, cell pellets with indicated genotypes or under indicated treatments were lysed in BC150 buffer (50 mM Tris-HCl, pH 7.3, 150 mM NaCl, 10% glycerol, and 1x protease inhibitor cocktail) and sonicated on ice for 30 seconds. After centrifugation, whole proteins were quantified with Bio-Rad Protein Assay Dye Reagent. 400 mg or 800 mg whole proteins were mixed with 225 μL VKH_2 generation reaction buffer containing 0.5% CHAPS (3-((3-cholamidopropyl) dimethylammonio)-1-propanesulfonate), 4 mM DTT and 100 μM MK4 at 37 °C for 1 hour. The reaction was stopped by the addition of 500 μL of pre-chilled 2-propanol. Next, 500 μL of n-hexanes was added for vitamin K extraction. After centrifugation at 5,000 g for 20 minutes at 4 °C, 500 μL of the organic phase was collected into new vials and dried under a gentle stream of nitrogen gas. The extracted metabolites were reconstituted in 500 μL methanol before measurement with LC-MS/MS.

VKH_2 detection by LC-MS/MS
The extracted VKH_2 and VK samples were separated using an Acquity UPLC CSH C18 column (2.1 × 100 mm, 1.7 μm) over an 8-minutes gradient elution on a Waters Acquity UPLC I-Class system. Mobile phase A was water with 5 mM ammonium formate, and mobile phase B was methanol, both containing 0.1% formic acid. After the injection, the gradient was held at 40% mobile phase B for 1 minute. And increased to 100% B in 3.8 minutes and stayed at 100% B for 2.7 minutes. The eluent composition returned to the initial condition in 0.2 minutes, and the column was re-equilibrated for an additional 1.3 minutes before the next injection was conducted. The oven temperature was set at 45 °C, and the flow rate was 400 μL per minute. The injection volume was 1 μL using the flow-through needle mode. The SYNAPT G2-Si -Q-ToF mass spectrometer was operated in positive electrospray ionization mode. A capillary voltage and sampling cone voltage of 1.2 kV and 30 V were used. The source and desolvation temperatures were kept at 120 and 500 °C, respectively. Nitrogen was used as the desolvation gas with a flow rate of 750L/h. The data were collected in duplicates over the mass range m/z: 50 to 650 Da in the sensitivity mode. The structural assignment of VKH_2 and VK in the samples was confirmed by matching the retention times and the fragmentation patterns with the standards. Data were acquired with MassLynx (version 4.1) software and processed with QuanLynx (version 4.1) software (Waters).

Vitamin K detection by ELISA assay
The total vitamin K levels were detected in samples of indicated genotypes or under indicated treatments using Human vitamin K ELISA Kit according to the manufacturer's protocol. For cell harvesting, cells at approximately 70% confluence were washed twice with 1×PBS and then quickly scraped with a cell lifter. 90% of the cells were transferred to Eppendorf tubes for vitamin K detection and 10% to the other Eppendorf tubes for protein quantification. Cells were centrifuged at 5,000 g at 4 °C for 5 minutes and resuspended in 1×PBS. Cells were then under freeze/thaw (dry ice/room temperature) cycle 3 times. After centrifugation at 1,500 g for 15 minutes, the supernatant was collected and subjected to detection. For tumor samples, 100-200 mg tumor samples were weighed, minced into small pieces, and homogenized in 1×PBS. The mixture was under freeze/thaw (dry ice/room temperature) cycle 3 times. After centrifugation at 1,500 g for 15 minutes, the supernatant was collected and subjected to detection.

Cell Metabolism
Article

CellPress

Lipid peroxidation analysis using C11-BODIPY

The day before the experiment, 12×10^4 cells were seeded in 6-well plate per well with cystine starvation, 4mM glutamate or warfarin, followed with adding vitamin K1 or K2. The next day, cells were treated with RSL-3 or TBH for the indicated time. Meanwhile, medium was added with vitamin K1 or K2. Then cells were labelled in 1×PBS containing 2 μM BODIPY 581/591 C11 dye for 30 minutes at 37°C. Subsequently, cells were trypsinized and rinsed by 1×PBS twice, resuspended in 500 μL 1×PBS, and strained through a 35 μm cell strainer (Falcon, 352235), following with flow cytometry analysis.

For xenograft-derived cells, tumor tissues were isolated from mice and immersed with 1×PBS in a plate. Further, tumor tissues were minced into small enough pieces and digested with collagenase type I (Thermo Figher, 17100017) at 37°C with intermittent mixing. After 1 hour incubation, minced tissues looked like a goopy mess and were pipetted to make live cells into single cell with gentle mechanical force. Then, the cells were strained with a 35 μm cell strainer, washed with 1×PBS twice and stained with 1× PBS containing 2 μM BODIPY 581/591 C11 dye for 25 minutes at 37°C. Then, the stained cells were washed by 1×PBS twice and resuspended 1×PBS for analysis.

Lipid peroxidation was assessed with Attune NxT Acoustic Focusing Cytometer through the BL1 channel (488nm) to obtain the oxidized lipid levels and the YL1 channel (561nm) to obtain reduced lipid levels. After obtaining the samples' oxidized C11 (oxC11) and reduced C11 (reC11) levels which are relative to the non-stained control, the lipid peroxidation ratio was calculated by oxC11/reC11*100%.

Mouse xenograft experiments

For xenograft of wildtype AsPC1 cells, 2.0×10^6 cells resuspended sterile PBS were mixed with Matrigel (Corning) at 1:1 ratio (v/v) and injected subcutaneously into *Nu/Nu* mice. 2 weeks later, the mice were assigned randomly into different treatment groups. Mice were orally administered with normal water, 6.6 μg/mL, or 13.2 μg/mL warfarin through bottled drinking water. Assuming water consumption every mouse (average 25g) is 3.75 mL every day, these two doses correspond to a warfarin uptake of 1 mg/kg or 2 mg/kg per mouse a day. For ferrostatin-1 (S7243, Selleck) treatment, 1mg/kg ferrostatin-1 was administered intraperitoneally per two-day per mouse for continuous 14 days. Mice were euthanized after 15 days of drug administration and tumors were dissected and weighed for further experiments.

For xenograft of KPCY cells, 5.0×10^5 cells resuspended sterile PBS were mixed with Matrigel (Corning) at 1:1 ratio (v/v) and injected subcutaneously into C57BL/6 mice. 10 days later, the mice were assigned randomly into different treatment groups. Mice were orally administered with normal water or 5.3 μg/mL warfarin through bottled drinking water. Assuming water consumption every mouse (average 20g) is 3.75 mL every day, these two doses correspond to a warfarin uptake of 1 mg/kg per mouse a day. Mice were euthanized after 15 days of drug administration and tumors were dissected and weighed for further experiments.

For xenograft of A375 NC re-expressing Empty Vector, NC re-expressing VKORC1L1, p53$^{-/-}$ re-expressing Empty Vector, or p53$^{-/-}$ re-expressing VKORC1L1, 4.0×10^6 cells resuspended sterile PBS were mixed with Matrigel (Corning) at 1:1 ratio (v/v) and injected subcutaneously into *Nu/Nu* mice. Mice were euthanized at 3 weeks after injection and tumors were dissected and weighed for further experiments.

QUANTIFICATION AND STATISTICAL ANALYSIS

Patients harbored with p53 mutation and relative *VKORC1L1* expression were analyzed from the UCSC Xena Platform. *VKORC1L1* genetic alteration data and the association of *VKORC1L1* genetic alteration with overall survival in patients with TCGA-PAN were derived from the cBioportal for Cancer Genomics databases (http://www.cbioportal.org/). The HTSeq-TPM RNA-seq expression data were retrieved from The TCGA (https://portal.gdc.cancer.gov). Kaplan–Meier survival curves for overall survival (months) were analyzed in R using Package 'survminer' and Package 'survival' with Log rank Mantel–Cox test method.[48] The "Gene Expression profile" module of the GEPIA2 web server was used to obtain box plots of the *VKORC1L1* expression difference in COAD, PAAD, and STAD between the tumor tissues and the corresponding normal tissues plus GTEx data, under the settings of *p-value* cutoff = 0.01, $|\log_2 FC|$ cutoff =1, and "No log scale". Western blot densitometry qualification was performed by ImageJ. Flow cytometry data were analyzed by FlowJo. Data were graphed using GraphPad Prism 8.0.

A two-tailed unpaired Student's t-test by GraphPad Prism 8.0 was done for the statistical analyses without specific statements. Data are presented as mean ± s.d. or mean ± SEM as indicated in Figure Legend. $p < 0.05$ was considered statistically significant between groups.